Department of Applied Physics

Computational study of isovalent group-V impurity doping and native point defects of III-V compound semiconductors

---

Ville Virkkala

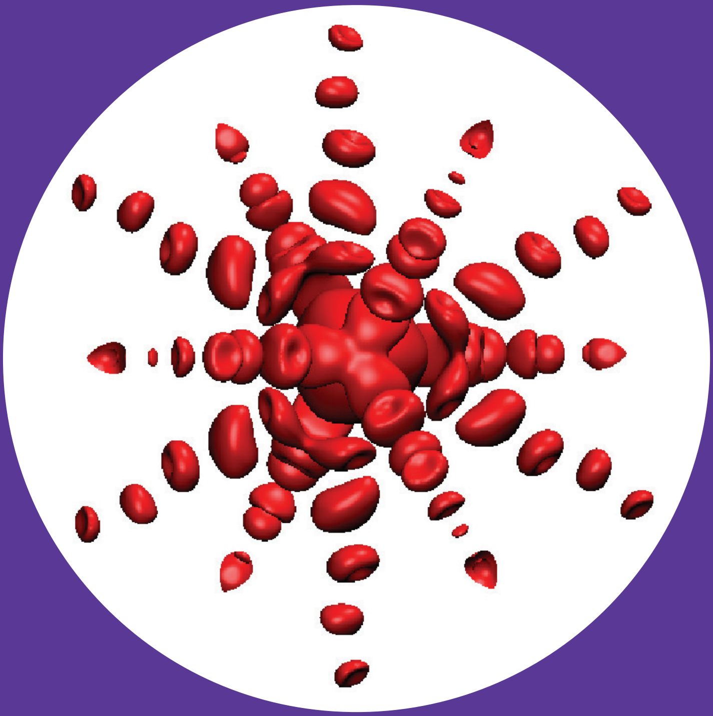

DOCTORAL
DISSERTATIONS

Aalto University publication series
DOCTORAL DISSERTATIONS 13/2014

Computational study of isovalent group-V impurity doping and native point defects of III-V compound semiconductors

Ville Virkkala

A doctoral dissertation completed for the degree of Doctor of Science in Technology to be defended, with the permission of the Aalto University School of Science, at a public examination held at the lecture hall E of the school on 14th of February 2014 at 13 o'clock.

Aalto University
School of Science
Applied Physics
COMP

Supervising professor
Prof. Martti Puska

Thesis advisor
D.Sc. Ville Havu

Preliminary examiners
Prof. Tapio Rantala, University of Tampere, Finland
D.Sc. Cristoph Freysoldt, Max-Planck-Institut für Eisenforschung,
Düsseldorf Germany

Opponent
Prof. Aron Walsh, University of Bath, England

Aalto University publication series
DOCTORAL DISSERTATIONS 13/2014

© Ville Virkkala

ISBN 978-952-60-5546-6
ISBN 978-952-60-5547-3 (pdf)
ISSN-L 1799-4934
ISSN 1799-4934 (printed)
ISSN 1799-4942 (pdf)
http://urn.fi/URN:ISBN:978-952-60-5547-3

Unigrafia Oy
Helsinki 2014

Finland

NORDIC ECOLABEL
441 697
Printed matter

Aalto University

Abstract

Aalto University, P.O. Box 11000, FI-00076 Aalto www.aalto.fi

Author
Ville Virkkala

Name of the doctoral dissertation
Computational study of isovalent group-V impurity doping and native point defects of III-V compound semiconductors

Publisher School of Science

Unit Department of Applied Physics

Series Aalto University publication series DOCTORAL DISSERTATIONS 13/2014

Field of research Computational Physics

Manuscript submitted 11 November 2013 **Date of the defence** 14 February 2014

Permission to publish granted (date) 14 January 2014 **Language** English

☐ **Monograph** ☒ **Article dissertation (summary + original articles)**

Abstract

In the 1990s it was observed that the optical properties of III-V compound semiconductors can be significantly modified by substituting the V component by just a small fraction of nitrogen causing the narrowing of the band gap of the material. This observation led to a huge interest towards these alloys. The interest stems from the fact that these materials can be used in high-efficiency solar cell applications by tuning the band gap of the alloy to harvest photons with certain energy as well as a base material for long-wavelenght lasers. Currently the most widely accepted theories explain the band gap narrowing with increasing nitrogen concentration by the interaction between the host material states and the nitrogen-induced states, which causes either the host material conduction band edge or nitrogen-induced states close to the bottom of the conduction band to shift into lower energies. However, it is also often suggested that the nitrogen-nitrogen interactions in these alloys lead to the broadening of the nitrogen-induced states which would then cause the band gap narrowing, even though the actual mechanism for the nitrogen-nitrogen interactions is unknown.

Alongside with the band gap engineering of III-V-N compound semiconductors, defects play a crucial role in the electrical properties in these materials. GaSb is a promising material for optoelectronic applications and undoped GaSb is known to be of *p*-type irrespective of growth conditions. The *p*-type conductivity is often connected to native point defects, but the origin of *p*-type conductivity is still largely debated.

The main result of this thesis is the development and implementation of a quantum mechanical model to describe the nitrogen-nitrogen interactions and the resulting broadening of the nitrogen-induced states in III-V compound semiconductors. The model is further extended to $GaAs_{1-x}Bi_x$ alloys. Our model reproduces qualitatively and quantitatively the experimentally observed band gap behavior as a function of nitrogen or bismuth concentration. In this thesis also the native point defect energetics in GaSb is studied using an advanced hybrid functional of the density functional theory. Special focus is given to an accurate treatment of charged defects by implementing a recently published correction scheme for electrostatic energy in periodic systems.

Keywords density functional theory, semiconductor, band gap engineering, dilute nitrides

ISBN (printed) 978-952-60-5546-6 **ISBN (pdf)** 978-952-60-5547-3

ISSN-L 1799-4934 **ISSN (printed)** 1799-4934 **ISSN (pdf)** 1799-4942

Location of publisher Helsinki **Location of printing** Helsinki **Year** 2014

Pages 97 **urn** http://urn.fi/URN:ISBN:978-952-60-5547-3

Aalto-yliopisto

Tiivistelmä

Aalto-yliopisto, PL 11000, 00076 Aalto www.aalto.fi

Tekijä
Ville Virkkala

Väitöskirjan nimi
Laskennallinen tutkimus III-V yhdistepuolijohteiden saostamisesta isovalenteilla ryhmän V epäpuhtausatomeilla ja itseispistevirheistä

Julkaisija Perustieteiden korkeakoulu

Yksikkö Teknillisen fysiikan laitos

Sarja Aalto University publication series DOCTORAL DISSERTATIONS 13/2014

Tutkimusala Laskennallinen fysiikka

Käsikirjoituksen pvm 11.11.2013 **Väitöspäivä** 14.02.2014

Julkaisuluvan myöntämispäivä 14.01.2014 **Kieli** Englanti

☐ **Monografia** ☒ **Yhdistelmäväitöskirja (yhteenveto-osa + erillisartikkelit)**

Tiivistelmä

1990-luvulla huomattiin, että III-V yhdistepuolijohteiden optisia ominaisuuksia voidaan merkittävästi muuttaa korvaamalla osa viidennen ryhmän atomeista typellä, jolloin materiaalin energia-aukko pienenee. Tämän havainnon vuoksi nämä materiaalit saivat osakseen paljon huomiota, koska niitä voitaisiin käyttää suuren hyötysuhteen aurinkokenno sovelluksissa säätämällä materiaalin energia-aukko keräämään tietyn energian fotoneita. Lisäksi säätämällä näiden materiaalien energia-aukko sopivaksi voitaisiin niitä käyttää pitkillä aallonpituuksilla toimivissa puolijohdelasereissa. Tällä hetkellä useimmissa teoreettisissa malleissa materiaalin energia-aukon pieneneminen typen määrän kasvaessa selitetään typen ja puolijohteen materiaalin tilojen välisellä vuorovaikutuksella, joka johtaa joko puolijohteen johtavuusvyön pohjan tai johtavuusvyön pohjan lähellä olevien typen tilojen siirtymiseen alemmille energian arvoille. Usein ilmiön on myös ehdotettu johtuvan typpiatomien välisien vuorovaikutuksien aiheuttamasta typen tilojen leviämisestä, vaikka tarkkaa mekanismia typpiatomien väliselle vuorovaikutukselle ei tunneta.

Energia-aukon säätämisen ohella myös pistevirheillä on merkittävä vaikutus III-V yhdistepuolijohteiden elektronisiin ominaisuuksiin. GaSb on lupaava materiaali optoelektroniikan sovelluksiin ja sen tiedetään olevan johtavuudeltaan aina p-tyyppistä riippumatta kasvatusolosuhteista. p-tyypin johtavuuden on usein esitetty liittyvän itseispistevirheisiin GaSb:ssä, mutta tästä on vielä paljon eriäviä mielipiteitä.

Tämän väitöskirjan merkittävin tulos on kvanttimekaanisen teorian kehittäminen ja toteuttaminen kuvaamaan typpiatomien välisiä vuorovaikutuksia III-V yhdistepuolijohteissa ja näistä johtuvaa typen tilojen leviämistä. Malli laajennettiin koskemaan myös $GaAs_{1-x}Bi_x$ seoksia. Työssä kehitetty malli ennustaa määrällisesti ja laadullisesti oikein energia-aukon suuruuden typen tai vismutin määrän funktiona verrattuna kokeellisiin tuloksiin. Tässä työssä tutkittiin myös GaSb:n itseispistevirheitä käyttämällä tiheysfunktionaaliteoriaa ja edistyksellistä hybridifunktionaalia. Työssä kiinnitettiin erityistä huomioita varattujen pistevirheiden mallintamiseen toteuttamalla äskettäin julkaistu sähköstaattisen energian korjausmenetelmä periodisissa rakenteissa.

Avainsanat tiheysfunktionaaltieoria, puolijohde, energia-aukon suunnittelu, laimeat nitridit

ISBN (painettu) 978-952-60-5546-6 **ISBN (pdf)** 978-952-60-5547-3

ISSN-L 1799-4934 **ISSN (painettu)** 1799-4934 **ISSN (pdf)** 1799-4942

Julkaisupaikka Helsinki **Painopaikka** Helsinki **Vuosi** 2014

Sivumäärä 97 **urn** http://urn.fi/URN:ISBN:978-952-60-5547-3

Preface

This thesis was conducted in the COMP unit of Aalto University during the years 2009-2013. The last two years of the research was founded by the Suomen Kulttuurirahasto Foundation. The computer time was provided by the CSC — the Finnish IT center for science.

Especially, I would like to thank my supervisor professor Martti Puska for providing me the opportunity to work with this project and for the great ideas and endless effort towards the articles of this thesis. I would like to also thank my instructor Ville Havu (D.Sc.) for the helpful discussions and support for my work as well as professor Filip Tuomisto for good ideas and encouragement to push my own ideas forward.

I thank Andris Gulans (D.Sc) and the other colleagues from the EPM group for the helpful discussions and the IT crew of the department for the IT support during my thesis work.

in Espoo, January 14, 2014,

Ville Virkkala

Contents

Preface i

Contents iii

List of Publications v

Author's Contribution vii

1. Introduction 1

2. Electronic structure of III-V compound semiconductors: effect of isovalent group-V impurity alloying and point defects 3
- 2.1 N alloyed III-V compound semiconductors: band gap tailoring 4
  - 2.1.1 Band anticrossing model for the large band gap bowing 6
  - 2.1.2 Replacing N with Bi 7
- 2.2 Point defects in III-V compound semiconductors 8

3. Applications in solar photovoltaic cells and long wavelength lasers 11
- 3.1 Multi-junction solar cells 11
- 3.2 Long wavelength lasers 13

4. Computational methods for ground state electronic structure calculations 15
- 4.1 Density functional theory 16
  - 4.1.1 Local density approximation 18
  - 4.1.2 Hybrid functionals 19
  - 4.1.3 Spin-orbit coupling in DFT calculations 20
- 4.2 Bloch theorem and the supercell approach 22
- 4.3 Formation energy calculations for point defects 23

4.3.1 Electrostatic finite-size effect correction for charged defects 23

5. Nitrogen and Bi induced modifications in the electronic structures of GaAs, GaP and GaSb 27

5.1 Substitutional nitrogen in GaAs and GaSb 27

5.2 N-N interactions in $\mathrm{GaAs}_{1-x}\mathrm{N}_x$ and $\mathrm{GaP}_{1-x}\mathrm{N}_x$ alloys and the band gap bowing 28

5.3 Bi induced modifications in the electronic structures of $\mathrm{GaAs}_{1-x}\mathrm{Bi}_x$ alloys 32

6. Hybrid functional study of native point defect energetics in GaSb 35

7. Conclusions 37

7.1 Developed theory to describe electronic structures of III-V-N alloy semiconductors 37

7.2 Generalization of the developed model to $\mathrm{GaAs}_{1-x}\mathrm{Bi}_x$ alloys 38

7.3 Native point-defect energetics in GaSb and the connection to p-type conductivity 38

A. Calculation of the matrix elements in the developed tight-binding method 41

Bibliography 43

Publications 49

List of Publications

This thesis consists of an overview and of the following publications which are referred to in the text by their Roman numerals.

I V. Virkkala, V. Havu, F. Tuomisto, M. J. Puska. Hybrid functional study of $GaAs_{1-x}N_x$ and $GaSb_{1-x}N_x$ alloys. *Physical Review B*, 85, 085134, February 2012.

II V. Virkkala, V. Havu, F. Tuomisto, M. J. Puska. Origin of the band gap bowing in $GaAs_{1-x}N_x$ and $GaP_{1-x}N_x$ alloys. *Physical Review B*, 88, 035204, July 2013.

III V. Virkkala, V. Havu, F. Tuomisto, M. J. Puska. Density functional theory study of $GaAs_{1-x}Bi_x$ alloys. *Physical Review B*, 88, 235201, December 2013.

IV V. Virkkala, V. Havu, F. Tuomisto, M. J. Puska. Native point defect energetics in GaSb: Enabling p-type conductivity of undoped GaSb. *Physical Review B*, 86, 144101, October 2012.

Author's Contribution

Publication I: "Hybrid functional study of GaAs$_{1-x}$N$_x$ and GaSb$_{1-x}$N$_x$ alloys"

The author had an active role in all parts of the research. Especially the author performed all the DFT calculations and wrote the first draft of the paper.

Publication II: "Origin of the band gap bowing in GaAs$_{1-x}$N$_x$ and GaP$_{1-x}$N$_x$ alloys"

The author defined the problem field and the framework for the research. The author also took active role in planning the developed tight-binding model and took care of the implementation of the model. The author solely did all the DFT calculations and wrote the matlab code to implement the developed tight-binding model. The author also wrote the first draft of the manuscript.

Publication III: "Density functional theory study of GaAs$_{1-x}$Bi$_x$ alloys"

The author defined the problem field and planned the research. The author did all the DFT and tight-binding calculations and wrote the first draft of the manuscript.

Publication IV: "Native point defect energetics in GaSb: Enabling p-type conductivity of undoped GaSb"

The author wrote the Fortran code for the electrostatic finite-size effect correction scheme and did all the DFT calculations. The author wrote the first draft of the manuscript.

1. Introduction

During the past decades there has been a huge technological evolution in the computer, mobile communication and information technologies [1]. This fast development has to a large extent based on a deep understanding on semiconductor physics and extremely advanced manufacturing methods of semiconductor components. Even though during the recent years, due to reaching the limit of the downsize scaling, the focus in theoretical research has shifted away from the basic semiconductors to novel materials like carbon nanotubes and graphene based materials, the band gap engineering and the defect control of conventional semiconductors is still under active theoretical and experimental research. Doping traditional III-V compound semiconductor materials, *e.g.*, with nitrogen opens new possibilities for optical telecommunications and high-efficiency solar cells [2, 3]. Recently, electron spin in silicon has been studied extensively as a possible realization of a spin qubit for quantum computing [4, 5].

Alongside with the rapid speed up of computer power also computational theories and methods have taken huge leaps. The foundations of quantum mechanics at the early 20th century [6] set the base for atomic scale calculations. The development of the density functional theory (DFT) [7, 8] in 1960s enabled calculations for complicated structures that can be solved by nowadays computers. The methods in the field of computational materials science provide sophisticated state of the art approaches for solving complicated many-electron problems from first principles, where the methods are derived directly from quantum mechanics. They provide a fast and cheap alternative for the experimental research and can open in research completely new viewpoints which could be otherwise difficult or impossible to achieve.

In this thesis, modifications of electronic structures of III-V compound semiconductors due to alloying by different group V atoms was studied using DFT. We also studied native point defect energetics and the impact of defects on the characteristic features, *i.e.*, the p-type conductivity, of the undoped GaSb. The main result of this thesis was the development and implementation of a quantum mechanical model to describe the N-induced modifications on the electronic structure of $\mathrm{GaAs}_{1-x}\mathrm{N}_x$ and $\mathrm{GaP}_{1-x}\mathrm{N}_x$ alloys, which was further extended to $\mathrm{GaBi}_{1-x}\mathrm{Bi}_x$ alloys. We also performed careful research for charged defects in GaAs and GaSb by implementing a recently published finite-size effect correction scheme [9, 10].

This thesis is organized as follows. In chapter 2 we review the current status of group V impurity alloyed III-V compound semiconductors and the underlying theory. In chapter 2 also a short summary of point defects in semiconductors is made. Chapter 3 presents applications of N doped III-V compound semiconductors in solar cells and long wavelength lasers. In chapter 4 the DFT methodology for ground state electronic structure calculations is reviewed and the supercell (SC) approach for point defect formation energy calculations is explained. In chapter 4 the implemented correction scheme for charged defects is also explained in detail. In chapters 5 and 6 the computational results for N and Bi alloyed III-V compound semiconductors, namely GaAs, GaSb and GaP, and native point defect energetics in GaSb are summarized. Finally chapter 7 is a concluding review of the main results of the dissertation and projects possible applications and future work.

2. Electronic structure of III-V compound semiconductors: effect of isovalent group-V impurity alloying and point defects

Semiconductors have laid the foundations of the modern information technology and solid state electronics. Elemental silicon is the most important semiconductor material and a superior choice for electronic devices due to its thermal properties, highly reliable processing techniques and cheap cost [1, 11]. However, due to its indirect band gap silicon has very poor optical properties [1]. Instead, GaAs is a binary III-V compound semiconductor which due to its direct band gap and excellent electron transport is a superior material for optoelectronic applications [1]. In this thesis the focus is on the binary III-V compound semiconductors: GaAs, GaP and GaSb.

The III-V compound semiconductors most commonly crystallize into a zinc-blende structure although exceptions can be found, *e.g.*, the wurtzite structure of GaN. The zinc-blende structure is composed of two interpenetrating face-centered cubic lattices of the two atom species. The other lattice is shifted 1/4 of the diagonal of the conventional cell with respect to the other one. Thus, in the zinc blende structure each atom has four nearest neighbors of the opposite type in a tetrahedral T_d configuration (see figure 2.1).

The key feature in semiconductors is that their conductivity can be greatly modified by doping them with impurity atoms. By doping the semiconductor with impurity atoms having more valence electrons compared to the host material atoms leads to n-type conductivity, *i.e.*, electrons are the charge carriers, and the impurity atoms are called donors. Instead, doping the semiconductor with impurities having less valence electrons leads to p-type conductivity, *i.e.*, holes are the charge carriers, and impurity atoms are called acceptors. However, in this thesis the isovalent doping of III-V compound semiconductors was studied, *i.e.*, impurity atoms have an equal number of valence electrons compared to the

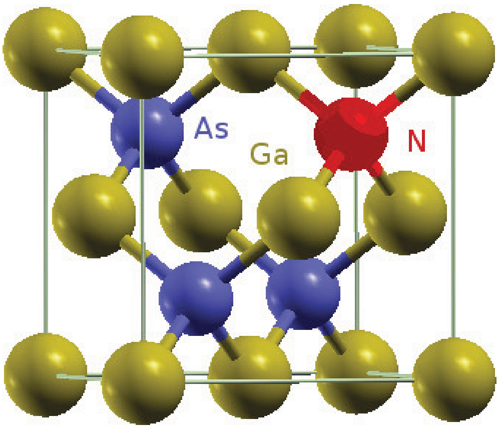

Figure 2.1. N atom substituting an As atom in GaAs in the zinc-blende structure. The figure is generated using the XCrySDen program [12].

substituted host material atoms. Especially the focus was on N and Bi alloying of these materials. Figure 2.1 shows as an example a N atom substituting an As atom in GaAs.

2.1 N alloyed III-V compound semiconductors: band gap tailoring

By inserting just a small fraction of N atoms into III-V compound semiconductors (around 0.1% in GaAs) already leads to significant modifications on the electronic structure of these materials. These modifications occur as band gap narrowing at low N concentrations [13] (<3%) and anomalously heavy effective electron masses which decrease with the increasing N concentration [14]. The band gap narrowing with increasing N concentration is in some sense counterintuitive because the band gap of GaN, $E_g = 3.27$ eV in zinc blende structure, is much wider than that of any of the conventional III-V compound semiconductors, *e.g.*, GaAs, GaP and GaSb.

Perhaps one of the earliest studies of N doped III-V compound semiconductors was performed by Thomas *et al.* in 1965 [15]. They studied N doped GaP and found that the characteristic features in the absorption and fluorescence spectra of GaP can be explained by an isolated substitutional nitrogen atom and nitrogen-nitrogen (NN_i) pairs at neighboring phosphorus sites. In the case of $GaAs_{1-x}N_x$ alloys the first observation of different N complexes was reported by Liu *et al.* as late as 1990 [16]. Here, x stands for the fraction of As sites occupied by N atoms with respect to all As sites. They performed luminescence measurements and forced by tuning the hydrostatic pressure the states related to NN_i pairs to enter into the band gap one after the other. These states then became the major exciton recombination channel. Later in 1990s it was realized that controlling the N concentration in GaAs can be used to decrease the band gap of GaAs [17]. This observation lead to a huge interest towards $GaAs_{1-x}N_x$ alloys. These alloys could be lattice matched to GaAs and due to their tunable band gap could be used in multi junction solar cells, where each junction is optimized to the wavelength of the light it collects [18]. During the past decade a large band gap narrowing, larger than that in GaAs, was reported in $GaSb_{1-x}N_x$ alloys [19]. This led to several experimental and computational studies of this alloy, because due to a direct, relatively small band gap, $GaSb_{1-x}N_x$ alloys show a large potential in fabricating long wavelength lasers.

Alongside with the observation of a decreasing band gap in N doped III-V compound semiconductors, theories trying to explain the origin of this phenomenon began to emerge. The first explanations came from the experimentalists [20] who suggested that the band gap reduction is due to an impurity band formation owing to N-N interactions. However, at late 1990s it was stated that the band gap reduction can be explained by the interaction between the N resonant state and the host material conduction band edge (CBE) [21]. This model, called the band anticrossing model (BAC) [21], soon became the most widely accepted model up to date (see below for details). Other popular schemes are based on the empirical pseudo-potential method [13]. In the method empirically corrected pseudopotentials, commonly adjusted to reproduce the experimental bulk band gaps [13], are used to solve the Schrödinger equation non-self-consistently for the system in question. Based on the empirical pseudopotential method Kent and Zunger concluded that the CBE formation in $GaAs_{1-x}N_x$ and $GaP_{1-x}N_x$ alloys involves interactions between the nitrogen-induced localized cluster states and the perturbed host states [22].

Despite huge expectations concerning N doped III-V compound semiconductors, fulfilled promises are not largely claimed up to date. This is mostly because the electronic properties of the bulk material, *e.g.*, the electron mobility significantly decreases due to N substitution [23]. The deteriorating electron mobility is often connected to the resonant-scattering from N complexes [24] and N-related defects. However, the origin of the poor electron mobility in these materials is still largely debated.

2.1.1 Band anticrossing model for the large band gap bowing

The BAC model was first introduced to explain the band gap narrowing in GaInNAs alloys by Shan *et al.* in Ref. [21]. Soon the model was extended to other III-V-N compound semiconductors such as $\mathrm{GaAs}_{1-x}\mathrm{N}_x$ [25] and $\mathrm{GaP}_{1-x}\mathrm{N}_x$ [26] as well as to II-VI semiconductor ternaries [27]. The BAC model is build above the Anderson impurity model [28] which describes the influence of atoms, having available inner shells, to electronic structures of metals.

According to the two-level BAC model, the N resonant state above the CBE of GaInAs and GaAs interacts with the host material CBE. This interaction is then treated as a perturbation leading to the eigenvalue problem [21]

$$\begin{vmatrix} E - E_M & V_{MN} \\ V_{MN} & E - E_N \end{vmatrix} = 0, \tag{2.1}$$

where E_M is the host CBE energy, E_N the energy of the N state and V_{MN} describes the interaction strength between the N state and the host CBE. The eigenvalue problem has the solution

$$E_{\pm} = \frac{E_N + E_M \pm \sqrt{(E_N - E_M)^2 + 4V_{MN}^2}}{2}. \tag{2.2}$$

Equation (2.2) has the appealing feature that it predicts the existence of the two states E_- and E_+. These states can be also verified experimentally [25, 21] and Eq. (2.2) can be forced to reproduce the measured E_- and E_+ states as a function of the N concentration, by adjusting the interaction term V_{MN} properly based on fitting the E_- and E_+ states to the experiments. The concentration dependence of V_{MN} is observed to have the form $\beta x^{\frac{1}{2}}$ [29].

In the case of $\mathrm{GaP}_{1-x}\mathrm{N}_x$ alloys it is well known that the N induced states are formed into the gap [13], below the host CBE, and the BAC model, assuming N states above the host CBE, cannot be directly applied. However, the problem is circumvented by assuming that now the N induced band in the gap is instead pushed downwards due to BAC interaction with the host CBE.

Despite the success of the BAC model to reproduce the experimental band gap behavior with respect to N concentration, the model is still largely debated. This is because the BAC model completely relies on fitting the theoretical E_- and E_+ states to the experimental ones and a very limited number of theoretical predictions can be drawn from the model.

Another struggling feature is the fact that computational studies, using periodic boundary conditions and thus actually modeling ordered alloys instead of random alloys, predict a rather linear band gap reduction as a function of the N concentration which is in contradiction with experiments [13, 30]. On the other hand, the BAC model predicts the same nonlinear concentration dependence for both the ordered and random alloys which is in a severe disagreement with the superior first principles calculations.

2.1.2 Replacing N with Bi

During the recent years the focus on research has gradually shifted from N alloying of III-V compound semiconductors to Bi alloying of these materials, in which a similar band gap narrowing is observed. This shift is related to the above-mentioned problems of manufacturing N doped materials with competent electronic properties. The problem is commonly suggested to be related to a large size mismatch between the N and As atoms and thus replacing N with Bi is often considered to be a solution [31].

In contrast to N-alloyed III-V compound semiconductors, the Bi induced states are formed into the valence band instead of the conduction band and the band gap narrowing is caused by the VBE upwards shift. Perhaps the first theoretical study considering Bi-doped GaAs was performed by Janotti *et al.* in Ref. [32] who predicted the existence of the hypothetical GaBi alloy, not yet realized in experiments, and suggested the Bi alloying of GaAs as a possible solution to manufacture 1 eV band gap materials for photovoltaic cells. Soon after this Fluegel *et al.* [33] reported a huge concentration-dependent spin-orbit (SO) splitting in $\mathrm{GaAs}_{1-x}\mathrm{Bi}_x$ alloys. In Ref. [34] it was noted that it may occur that the SO splitting energy becomes larger than the band gap in $\mathrm{GaAs}_{1-x}\mathrm{Bi}_x$ alloys. This phenomenon, together with a large band gap, could provide new opportunities for near-infrared laser due to a suppression of the Auger recombination processes from the valence band edge (VBE) into the CBE. Recent photomodulated spectroscopy measurements by Kudrawiec *et al.* [35] have further enlightened the nature of VBE and the SO splitting in $\mathrm{GaAs}_{1-x}\mathrm{Bi}_x$ alloys. They found that due to Bi incorporation of 3% the E_0 transition from the top of the VBE to the bottom of the conduction band significantly broadens compared to that of the $E_0 + \triangle_{SO}$ transition from the spin split-off band to the bottom of the conduction band. They also observed a large red shift for the E_0 transition, while the $E_0 + \triangle_{SO}$ transition was found to be rather insensitive, indicating that the large SO splitting is due to the upwards shift of the valence band maximum (VBM).

Alberi *et al.* explained the narrowing of the band gap of $\mathrm{GaAs}_{1-x}\mathrm{Bi}_x$ alloys using the valence band anticrossing model (VBAC) [36]. In this model the localized Bi state in $\mathrm{GaAs}_{1-x}\mathrm{Bi}_x$ interacts with the host material VBE, pushing it upwards causing the band gap reduction. However, in contrast to $\mathrm{GaAs}_{1-x}\mathrm{N}_x$ alloys, theoretical studies up to this day do not clearly confirm the existence of localized Bi states in the valence band [37, 38]. Instead it is suggested that the Bi states should be viewed as a strongly perturbed host states [38].

2.2 Point defects in III-V compound semiconductors

In a perfect crystal each atom has a strictly defined position in a three-dimensional periodic lattice. Imperfections are deviations from this perfect three-dimensional array and they are crucial for the mechanical and electrical properties of the material. These imperfections in the perfect three-dimensional periodic crystal can be divided into lattice defects and impurities (foreign atoms). There are zero-dimensional (point), one-dimensional (line) and two-dimensional (planar) lattice defects [39]. Point defects consists only of one or a few atoms while one-dimensional defects are line defects like edge dislocations. Planar defects are for example grain boundaries or antiphase boundaries [39]. However, in this thesis the only lattice defects considered are the point defects in III-V compound semiconductors.

There are three main types of point defects in a compound semiconductor of type AB: a **vacancy** defect is formed when a normally occupied lattice site is vacant, an **interstitial** defect is a defect that occupies a normally unoccupied site in the lattice and an **antisite** defect is a defect were an atom of type A occupies a site of atom B, or vice versa. Also more complex defect structures can exist, like a vacancy antisite pair or a split-interstitial. Impurities can be intentional or unintentional. Intentional substitution of impurities in the host semiconductor is called as doping and it is the key factor in semiconductor technology, whereas detrimental impurities can be unintentionally incorporated during the growth process.

Creating a defect into a perfect structure always requires energy. However, the creation of a defect also increases the entropy of the system and

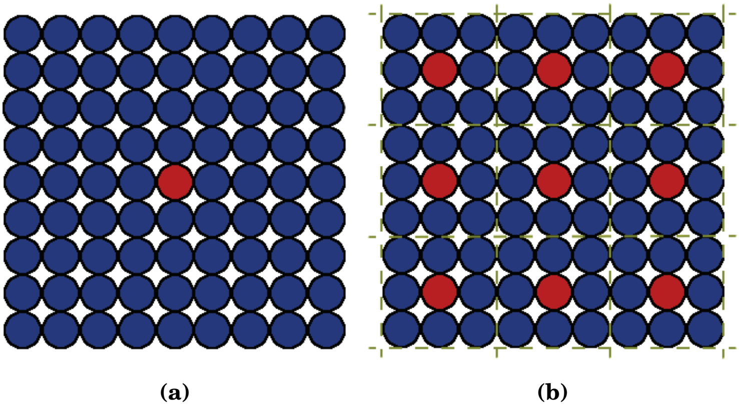

Figure 2.2. Example of an isolated defect (a) and a defect in the SC approximation (b). The red circles represent the defect and the blue circles the bulk material. The dashed lines in (b) represent the SC boundaries.

thus formation of a defect may lower the Gibbs free energy

$$G = H - TS, \tag{2.3}$$

where H is the enthalpy, T the temperature and S is the entropy. Thus, the Gibbs free energy can have a minimum at a finite defect concentration and the equilibrium defect concentration is obtained from the thermodynamics [39]. In defect calculations the key quantities obtained are the formation energies and the charge transition levels. The defect calculations are commonly performed within the DFT framework using the SC approximation. The SC is periodically repeated over the whole space and to prevent the defect from interacting with its own periodic images the defect in question must be surrounded by a large enough number of host material atoms. This structure is called as the SC. The concept of SC is illustrated in figure 2.2 in the case of a single defect in a SC. The SC approach is particularly popular, because it allows the use of various techniques popular in computational material science. Especially, in the SC approach plane waves are a natural choice for the basis functions in the numerical solution due to the Bloch's theorem [40] and the problem can be transformed efficiently into the reciprocal space using the fast Fourier transform. The DFT methodology to calculate the formation energies of point defects is explained in detail in section 4.3.

3. Applications in solar photovoltaic cells and long wavelength lasers

3.1 Multi-junction solar cells

The operation principle of a single $p-n$ junction solar cell is based on the creation of an electron-hole pair. An electron-hole pair is created when a photon of the energy E_ν larger than the band gap E_g of the solar cell semiconductor material excites an electron from the material valence band into the conduction band leaving a hole in the valence band [41]. A single junction $p-n$ solar cell is formed by bringing into a contact n- and p-type semiconductor materials. The Resulting $p-n$ junction allows the electrons photo excited to travel only in one direction across the junction, from the p side to the n side, and the holes in the opposite direction. By bringing an external load into contact with the solar cell through external leads allows the electrons to travel from the n side through the load back to the p side, where they recombine with the holes. A schematic illustration of the solar cell operation is shown in figure 3.1(a).

The solar cell efficiency is limited by the fact that only photons with energies $E_\nu > E_g$ can create electron-hole pairs while photons of smaller energy are lost in the sense of energy harvesting. Also the photon energy exceeding the band gap energy is lost as heat. Thus only a part of a visible light, composed of photons with different energies, can be utilized in a single junction solar cell. For a single $p-n$ junction solar cell the maximum efficiency is limited by the Shockley-Quisser (SQ) limit [42], which describes the energy conversion efficiency of the sunlight into electrical energy. The SQ limit for the most widely used silicon solar cells is around 29% [43]. To overcome the SQ limit of the single junction solar cells more advanced solar cell architectures have been developed during the years. Especially, important are the multi junction solar cells (described below)

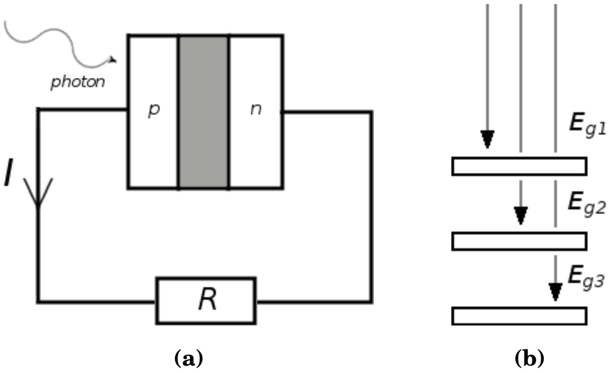

(a) **(b)**

Figure 3.1. Schematic illustration of a single $p-n$ junction solar cell operation (a). Geometry of a multi junction solar cell (b). In (a) the grey area indicates the depletion region. In (b) band gaps E_g decrease from top to bottom, *i.e.*, $E_{g1} > E_{g2} > E_{g3}$.

and the best efficiencies to date have been achieved using these multi junction solar cells [41, 18].

In multi junction solar cells several materials with different band gaps are connected in series in a stacked manner (see figure 3.1(b)), with the materials band gap decreasing from the top to the bottom of the stack [41]. The idea in the multi junction solar cell is that the band gap of each material layer is tuned to harvest photons of a certain energy range. Thus, multi junction solar cells can greatly improve the efficiency compared to single junction solar cells by harvesting photons from a much larger energy range. In the multi junction approach the theoretical efficiency is raised up to 86% in the case of infinitely many layers and concentrated sunlight [44].

The first monolithic (junctions connected in series) multi junction solar cells in production for space applications consisted of three layers GaInP/GaAs/Ge. A clearly better efficiency was projected for three- and four-junction solar cell structures based on III-V compound semiconductors and by requiring materials with band gaps smaller than that of GaAs [45]. That is why the observation by Weyers *et al.*, claiming that the band gap of GaAs can be reduced by substituting just a small fraction of As atoms by N atoms [17] (see section 2.1), attained a considerable attention, because these alloys could provide the needed band gaps with the optimal lattice constant. Soon the GaInNAs became the most prominent material in multi-junction solar cell applications [18]. However, the expectations for N alloyed III-V compound semiconductors in the solar cell applications are still not largely fulfilled. This is because the N-alloyed III-V-based multi-junction devices suffer from short minority carrier diffusion lengths, the roots of which are still unknown. Long diffusion lengths are essential for high-efficiency solar cells to efficiently collect the photogenerated carriers [18].

Very recently the Fraunhofer Institute for Solar Energy Systems and the collaborators launched a press release for a new world record in solar cell efficiency of 44.7 % at 297 suns [46]. The world record was obtained using a four-junction III-V multi-junction solar cells. In the manufacturing process an advanced wafer bonding technique was used which allows high-quality connection of two semiconductor crystals, which cannot be otherwise matched. However, the details of the used III-V semiconductor materials was not given in the press release.

3.2 Long wavelength lasers

The data transmission distance in a fiber network reduces as the transmission rate increases. For example for the standard 850 nm wavelength vertical cavity surface-emitting lasers (VCSEL) the transmission distance decreases from 7-8 km down to about 50 m, when the data transmission rate increases from 100 Mbps to 10 Gbps [2]. The 50 m transmission distance is simply too small to be used in any practical optical network. However, for optical networks operating with long wavelengths of 1.3 or 1.55 μm the transmission distance may be several kilometers with the 10 Gbps transmission rate [2]. With these wavelengths the pulse dispersion and absorption losses are minimized in silica-based optical fibers [47]. Thus there is a huge interest towards VCSELs operating with wavelengths of 1.3 or 1.55 μm.

Lasers operating at wavelengths of 1.3 or 1.55 μm can be manufactured using InGaP or InGaAlAs grown on the InP substrate [2, 48]. However, there are significant drawbacks in the case of VCSELs, related to thermal and optical gain properties, with these materials. Thus, significant advances would be gained if VCSEL lasers could be manufactured on a GaAs substrate. That is because in the case of GaAs the standard 850 nm VCSEL structure could be utilized, resulting in an easier manufacturing process, better optical and electronic confinements and a monolithic growth process [2, 48]. To manufacture VCSEL lasers on GaAs requires materials with band gaps from 0.78 to 0.95 eV lattice matched to GaAs [2]. Finding such an alloy was long considered to be impossible until Weyers *et al.* [17] discovered that the band gap of GaAs reduces with the increasing N concentration. Up to this day several reports have described lasers operating at around the 1.3 μm wavelength, grown on GaAs substrate and utilizing the GaInNAs alloys as the material with the band gap smaller than 1 eV [49, 50].

4. Computational methods for ground state electronic structure calculations

The starting point for the electronic structure calculations is the many-body Schrödinger equation for both nuclei and electrons [51]

$$\begin{aligned} \hat{H} &= -\frac{\hbar^2}{2m_e}\sum_i \nabla_i^2 + \sum_{i,I}\frac{Z_I e^2}{|\mathbf{r}_i - \mathbf{R}_I|} + \frac{1}{2}\sum_{i\neq j}\frac{e^2}{|\mathbf{r}_i - \mathbf{r}_j|} \\ &\quad -\sum_I \frac{\hbar^2}{2M_I}\nabla_I^2 + \frac{1}{2}\sum_{I\neq J}\frac{Z_I Z_J e^2}{|\mathbf{R}_I - \mathbf{R}_J|}, \end{aligned} \tag{4.1}$$

where lowercase subscripts stand for electrons and uppercase subscripts for nuclei. Above, $\hbar$ is the reduced Planck constant, e is the elementary charge, Z_I is the number of protons in nucleus I and m_e, M_I are the masses of an electron and a nucleus I, respectively. However, solving Eq. (4.1) even for a small number of atoms, not to speak of real systems, is a formidable tasks and approximations are required. The first and perhaps the most important one is the Born-Oppenheimer approximation. In this approximation the nuclear kinetic energy, *i.e.*, the fourth term in Eq. (4.1), is considered to be negligible and it is omitted. Further, the whole system wave function is separated into nuclear and electronic parts and the electronic part is considered to depend on the nuclei only parametrically. Thus, one obtains the Schrödinger equation for the electrons

$$\begin{aligned} \hat{H}_e\Psi_e &= (-\frac{\hbar^2}{2m_e}\sum_i \nabla_i^2 + \sum_{i,I}\frac{Z_I e^2}{|\mathbf{r}_i - \mathbf{R}_I|} + \frac{1}{2}\sum_{i\neq j}\frac{e^2}{|\mathbf{r}_i - \mathbf{r}_j|} \\ &\quad +\frac{1}{2}\sum_{I\neq J}\frac{Z_I Z_J e^2}{|\mathbf{R}_I - \mathbf{R}_J|})\Psi_e \\ &= E_e\Psi_e. \end{aligned} \tag{4.2}$$

In the case of non-interacting electrons, solving Eq. (4.2) is a relatively easy task and even analytic expressions can be found for non-interacting electron gas. However, the reason that makes solving of Eq. (4.2) extremely cumbersome, is the fact that electrons are correlated with each other through the Coulomb potential. Thus, finding numerical methods for solving Eq. (4.2) has evolved to real state of the art methods since the early decades of the 20th century.

The first methods for solving Eq. (4.2) numerically were the Hartree-Fock (HF) like methods. In these methods the multi-electron wave function is approximated by a correctly anti-symmetrized Slater determinant of single electron orbitals. The unknown single-electron orbitals are then calculated from the HF equations [6] obtained through the variational principle. The problem of the HF method is that it completely neglects the electron-electron Coulomb correlation. To overcome this deficiency several post-HF methods have been developed during the years. One popular approach is the Møller-Plesset perturbation theory, where the electron-electron Coulomb correlation is treated as a small perturbation [52].

Regardless of the success of the HF methods, the real breakthrough in the electronic structure calculations was the DFT, the predecessor of which was the Thomas-Fermi model [51]. DFT was sparked by the Hohenberg-Kohn theorem [7] published in 1964 which set the foundings of the theory. This theorem states that all the ground state properties of the system are uniquely determined by the ground state electron density. However it was the Kohn-Sham equations [8] which made the DFT applicable to electronic structure calculations. The DFT method is discussed in more detail in the next section.

Nowadays there exist various *ab initio* electronic structure codes utilizing state of the art methods for solving the Kohn-Sham equations. These methods include the SC approximation, pseudopotential approach, Brillouin zone integration and the projector-augmented wave method [53]. In this thesis the ground state electronic structure calculations are performed using the Vienna *ab initio* simulation package (VASP) [54].

4.1 Density functional theory

The key idea in time independent DFT is to replace the complicated many-body problem of interacting particles, with the simplified one of non-interacting particles. The missing correlation and exchange part of the simplified problem is then completed by an exchange-correlation functional. In the Hartree atomic units, in which $m_e = e = \hbar = 1/(4\pi\epsilon_0) = 1$, the DFT energy functional for a system of N electrons reads as [51]

$$\begin{aligned} E[n] &= \sum_i^N \int \psi_i^* \left(-\frac{1}{2}\right) \nabla^2 \psi_i d\mathbf{r} + \int n(\mathbf{r}) V_{\text{ext}} d\mathbf{r} \\ &+ \int \int \frac{n(\mathbf{r})n(\mathbf{r}')}{|\mathbf{r}-\mathbf{r}'|} d\mathbf{r}' d\mathbf{r} + E_{XC}[n(\mathbf{r})] + E_{II}. \end{aligned} \tag{4.3}$$

Above, the first term is the kinetic energy of the non-interacting electron system, the second term accounts for the interaction between the electrons and the external potential (normally due to the nuclei, the second term in Eq. (4.2)), the third term is the Hartee energy of electrons, the fourth term, E_{XC}, is the exchange-correlation energy and the last term is the interaction energy between the nuclei (*i. e.*, the last term in Eq. (4.2)).

The electron density $n(\mathbf{r})$ is obtained from the single electron orbitals ψ_i as

$$n(\mathbf{r}) = \sum_i^N |\psi_i|^2, \tag{4.4}$$

The orbitals ψ_i minimizing the energy functional of Eq. (4.3) are obtained by varying Eq. (4.3) with respect to the ψ_i^* under the constraint $\int \psi_i^*(\mathbf{r})\psi_j(\mathbf{r})d^3\mathbf{r} = \delta_{i,j}$. This leads to the Kohn-Sham equations [8]

$$\left(-\frac{1}{2}\nabla^2 + V_{ext}(\mathbf{r}) + V_H(\mathbf{r}) + V_{XC}(\mathbf{r})\right)\psi_i(\mathbf{r}) = \epsilon_i \psi_i(\mathbf{r}), \tag{4.5}$$

where V_H is the Hartree potential of electrons

$$V_H(\mathbf{r}) = \int \frac{n(\mathbf{r}')}{|\mathbf{r}-\mathbf{r}'|} d\mathbf{r}' \tag{4.6}$$

and V_{XC} is the exchange-correlation potential

$$V_{XC}(\mathbf{r}) = \frac{\delta E_{XC}[n(\mathbf{r})]}{\delta n(\mathbf{r})}. \tag{4.7}$$

The Kohn-Sham equations must be solved self-consistently and the general procedure is to start with a guessed initial electron density $n(\mathbf{r})$. The orbitals ψ_i are then solved from Eq. (4.5) and the energy functional Eq. (4.3) is evaluated. The new electron density is obtained from Eq. (4.4) and the new orbitals ψ_i are solved. This procedure is repeated until the convergence of the energy is obtained. The self-consistent cycle above can be accelerated by mixing the electron densities from the current and previous steps of the cycle and using efficient matrix diagonalization schemes for the Kohn-Sham-Hamiltonian (Eq. (4.5)) [54]. It is also possible to directly minimize the energy functional Eq. (4.3) instead of the self-consistent cycle [55].

The Kohn-Sham scheme is in principle exact. However, the exact form of the exchange-correlation functional is unknown and approximations are needed.

4.1.1 Local density approximation

In local density approximation (LDA) the exchange-correlation energy per electron $\epsilon_{xc}(n(\mathbf{r}))$ at a given point depends only on the electron density at that point. Thus the exchange-correlation energy is obtained as an integral

$$E_{xc}[n] = \int n(\mathbf{r})\epsilon_{xc}(n(\mathbf{r}))d\mathbf{r}. \tag{4.8}$$

In LDA the exchange-correlation energy per electron can be decomposed into exchange and correlation part

$$\epsilon_{xc}(n(\mathbf{r})) = \epsilon_x(n(\mathbf{r})) + \epsilon_c(n(\mathbf{r})). \tag{4.9}$$

The analytic form of the exchange part is taken to be that of a homogeneous electron gas [51]. However, the analytic form of the correlation part is unknown, except at the low- and high-density limits, and various analytical expressions for the correlation part has been developed during the years [56, 57].

In general LDA should work well for the systems with slowly varying electron densities resembling the homogeneous electron gas. The obvious deficiency in LDA are the spurious self-interaction terms, *i.e.*, the electron interacts with itself so that the self-Hartree and self-exchange-correlation energies are not exactly cancelled by the non-local exchange interaction in the HF approximation. In addition, there is a depletion of the electron density around a given electron, called as the exchange-correlation hole, due to the exchange and correlation effects. In LDA the exchange-correlation hole is spherically symmetric [58] while in real systems this is not true. Despite these evident deficiencies LDA works surprisingly well also in many inhomogeneous systems with rapidly decaying electron densities. The reason for this is that the exact exchange-correlation energy depends only on the spherical average of the exchange-correlation hole and the hole should contain exactly one charge unit [58]. The spherical LDA exchange-correlation hole resembles that of the spherical average of the real exchange-correlation hole and it also fulfills the above mentioned sum rule [58].

The success of LDA has led to many schemes in which LDA is only moderately corrected in a (semi) local manner. Among them the generalized gradient approximation (GGA) is the most common. In GGA the exchange-correlation functional also depends on the gradient of the density, which should better take into account the slow variations in the electron density.

4.1.2 Hybrid functionals

The idea of the hybrid functionals is to substitute a part of the DFT exchange by the exact HF exchange. The first practical formulation of the hybrid functional approach was given by Becke [59], who wrote the exchange energy functional as a linear interpolation between the noninteracting and fully-interacting systems in the form

$$E_{xc} = \frac{1}{2}E_x + \frac{1}{2}U_{xc}^{LDA}, \tag{4.10}$$

where E_x is the pure exchange energy of the Kohn-Sham Slater determinant and U_{xc}^{LDA} is the energy corresponding to the LDA exchange-correlation [59]. The problem with this approach is a huge computational cost and a poor performance with metallic systems [60]. These problems originate from the slow decay of the HF exchange, which also depends on the band gap of the material.

To overcome the above mentioned deficiencies Heyd *et al.* [60] introduced the so-called screened hybrid functional. The idea of the screened hybrid-functional is to replace a portion of the short-range DFT exchange by a short-range HF exchange. This is achieved by decomposing the Coulomb operator of the HF exchange into short- and long-range parts using the screening parameter ω

$$\frac{1}{r} = \frac{\mathrm{erfc}(\omega r)}{r} + \frac{\mathrm{erf}(\omega r)}{r}, \tag{4.11}$$

where the first term is the short-range part of the HF exchange and the second term is the long-range part. In above erf and erfc are the error and complementary error functions, respectively. The exchange-correlation energy is then calculated as [60]

$$\begin{aligned} E_{xc}^{HSE} &= aE_x^{\mathrm{HF,SR}}(\omega) + (1-a)E_x^{\mathrm{PBE,SR}}(\omega) \\ &\quad + E_x^{\mathrm{PBE,LR}}(\omega) + E_c^{\mathrm{PBE}}. \end{aligned} \tag{4.12}$$

Above, the parameter a determines the portion of the short-range HF exchange and it is called as the HF mixing constant. The PBE stands for the PBE functional which is one of the GGA functionals [61]. The short range DFT exchange is obtained by scaling the PBE exchange-correlation hole by the short-range Coulomb screening factor and the long-range DFT exchange is obtained as $E_x^{\mathrm{PBE,LR}}(\omega) = E_x^{\mathrm{PBE}} - E_x^{\mathrm{PBE,SR}}(\omega)$ [60]. The HF mixing constant a can be evaluated to be $1/4$ according to the perturbation theory [62]. However, a more common practice to determine the HF mixing constant is to adjust it so that the calculated band gap of the system in question agrees its experimental value [63].

Even in the case of screened hybrid functionals the calculations are computationally much heavier compared to calculations done with the local functionals. In Ref. [64] Kuisma *et al.* derived a computationally efficient method based on GLLB approximation [64, 65]. In this method the exchange-correlation potential is divided into screening and response parts. In Ref. [64] the screening part was evaluated using a modified PBE functional and the exchange response part was evaluated analogous to Ref. [65]. In Ref. [64] the method was found to significantly improve the calculated band gaps while being computationally as fast as the GGA approximation.

4.1.3 Spin-orbit coupling in DFT calculations

The SO coupling is a relativistic effect and it couples the electron spin into its own orbital motion. The SO coupling is especially important for heavy element systems in which electron velocities become relativistic. In solids the SO coupling modifies the band structures of materials by removing state degeneracies near the Fermi level. For example in the case of GaAs the SO coupling separates the heavy and light hole bands at the VBE and a split-off band occurs at a lower energy. This is evident from figure 4.1 where DFT band structures are shown in GaAs in the case of a 2-atom unit cell with and without the SO coupling.

For a hydrogenic atom the relativistic electron Hamiltonian can be approximated to be of the form [6]

$$H = H_0 + H_{\text{kin}} + H_{\text{dar}} + H_{\text{SO}}. \tag{4.13}$$

Above, H_0 is the non-relativistic Hamiltonian and H_{kin} is the relativistic kinetic energy correction obtained from the relativistic momentum-energy relation

$$H_{\text{kin}} = -\frac{\mathbf{p}^4}{8m^3c^2}, \tag{4.14}$$

where m is the electron mass and c the speed of light. Further, H_{dar} is the Darwin correction obtained from the Dirac equation [6]

$$H_{\text{dar}} = \frac{\hbar^2}{8m^2c^2}\nabla^2 V, \tag{4.15}$$

where V is the potential energy due to the nucleus. Finally H_{SO} is the SO coupling term obtained from the Dirac equation [6]

$$H_{\text{so}} = \frac{1}{2m^2c^2}\frac{1}{r}\frac{d}{dr}V(r)\mathbf{L}\cdot\mathbf{S}, \tag{4.16}$$

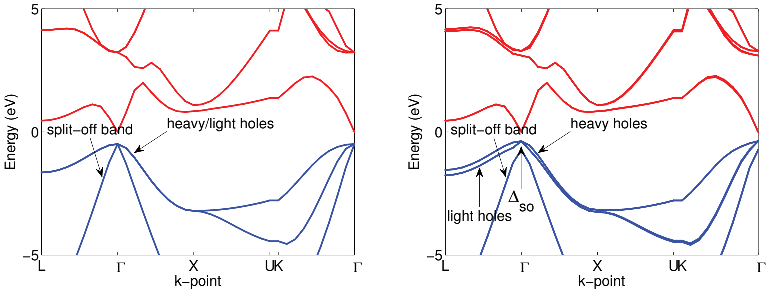

(a) **(b)**

Figure 4.1. DFT calculated band structure in GaAs in the case of 2-atom unit cell without SO coupling (a) and with SO coupling (b).

where **L** and **S** are the angular and spin momenta respectively. In Ref. [66] MacDonald *et al.* derived a fully relativistic augmented-plane-wave method, starting from the radial Dirac equation. A similar approach is used in the VASP code and the relativistic effective potential is divided into a diagonal part containing the relativistic kinetic energy correction and the Darwin correction, the scalar relativistic part, and the SO operator [67].

Due to the SO coupling the electron wavefunctions become spinors, *i.e.*,

$$\psi_i^\alpha(\mathbf{r}) = \varphi_i \chi^\alpha, \tag{4.17}$$

where χ^α is a two-component spinor. The 2x2 density matrix is then obtained as

$$n_{\alpha\beta}(\mathbf{r}) = \sum_i \psi_i^\alpha \psi_i^{\beta *}. \tag{4.18}$$

The Hamiltonian also becomes non-diagonal in spin and the DFT calculations must be performed in the noncollinear mode. In the VASP code [54] the electron density is obtained as a trace of density matrix $n^{\alpha\beta}(\mathbf{r})$ in the noncollinear mode [68]

$$n_{\mathrm{Tr}}(\mathbf{r}) = \sum_\alpha n_{\alpha\alpha}(\mathbf{r}). \tag{4.19}$$

The 2x2 density matrix can be also written as

$$n_{\alpha\beta}(\mathbf{r}) = [n_{\mathrm{Tr}}(\mathbf{r})\delta_{\alpha\beta} + \vec{m}(\mathbf{r}) \cdot \vec{\sigma}_{\alpha\beta}]/2, \tag{4.20}$$

where, $\vec{m}(\mathbf{r})$ is the magnetization density and $\vec{\sigma} = (\sigma_x, \sigma_y, \sigma_z)$ where $\sigma_x, \sigma_y, \sigma_z$ are the Pauli spin matrices. The magnetization density $\vec{m}(\mathbf{r})$ is obtained as

$$\vec{m}(\mathbf{r}) = \sum_{\alpha,\beta} n_{\alpha\beta}(\mathbf{r}) \cdot \vec{\sigma}_{\alpha\beta}. \tag{4.21}$$

4.2 Bloch theorem and the supercell approach

Solving Eq. (4.2) in the DFT framework still requires solving the electron wavefunctions for infinitely many electrons extended over the whole crystal lattice [40]. However the problem is made solvable by the Bloch's theorem [40].

The Bloch theorem states that in a periodic lattice with the periodic potential $U(\mathbf{r}+\mathbf{L}) = U(\mathbf{r})$, where $\mathbf{L}$ is a lattice vector, an electron wave function can be written in the form

$$\psi_k(\mathbf{r}) = e^{i\mathbf{k}\cdot\mathbf{r}} u_k(\mathbf{r}), \tag{4.22}$$

where $u_k(\mathbf{r})$ has the periodicity of the Bravais lattice. The $\mathbf{k}$ indicates the wave vector and it can be restricted into the first Brillouin zone. Because $u_k(\mathbf{r})$ is periodic in $\mathbf{L}$ it can be written as a Fourier series in the form

$$u_k(\mathbf{r}) = \sum_{\mathbf{G}} c_{k,G} e^{i\mathbf{G}\cdot\mathbf{r}}, \tag{4.23}$$

where $\mathbf{G}$ is a reciprocal lattice vector. Thus the electronic wave function can be written as a sum of plane waves in the form [40]

$$\psi_k(\mathbf{r}) = \sum_{\mathbf{G}} c_{k+G} e^{i(\mathbf{k}+\mathbf{G})\cdot\mathbf{r}}. \tag{4.24}$$

The Bloch theorem transforms the problem of infinitely many electrons with wave functions extending to infinity into a problem of infinitely many k-points within the first Brillouin zone [40]. The problem of infinitely many k-points can be circumvented by noticing that the wave function changes only little between two k-points close to each other. Thus, in calculations it is enough to choose only a limited number of k-points within the first Brillouin zone. The further consequence of the Bloch theorem is that the energy levels of an electron are functions of $\mathbf{k}$ having the periodicity of the reciprocal lattice, *i.e.*, $E_n(\mathbf{k}+\mathbf{G}) = E_n(\mathbf{k})$ [69]. Here n is the band index. The functions $E_n(\mathbf{k})$ are known as the band structure which is one of the most important properties characterizing the solid.

A typical approach in DFT calculations is to choose a specific geometry with a limited number of atoms, which as periodically repeated fills the whole space, and perform the calculation within this geometry. In the case of bulk calculations the geometry can be chosen to be the primitive cell of the system. For example in the case of GaAs with the zinc-blende structure, the primitive cell contains only two atoms and the system can be solved with ease within the DFT formalism.

4.3 Formation energy calculations for point defects

In the SC approximation (see sections 2.2 and 4.2) the defect formation energy is calculated as [70]

$$\begin{aligned} E^f &= E_{\text{tot}}[\text{def}+\text{bulk}] - E_{\text{tot}}[\text{bulk}] - \sum_i n_i \mu_i \\ &\quad + q(E_v + E_f) - \Delta E. \end{aligned} \tag{4.25}$$

Above, $E_{\text{tot}}[\text{def}+\text{bulk}]$ and $E_{\text{tot}}[\text{bulk}]$ are the energies of the defect and bulk SCs, respectively, E_v is set equal to the valence band maximum (VBM), E_f is the Fermi level referenced to the VBM. Further, n_i is the number of removed (a negative number) or added (a positive number) atoms of type i and μ_i is the chemical potential of atom of type i which is added or removed. The method to calculate the chemical potentials is explained in the case of GaSb in section 6. The last term ΔE is an energy correction term, discussed below, which accounts for the spurious interactions between a charged defect and its periodic images, which need to be taken into account to get the correct isolated defect formation energy.

In formation energy calculations for point defects one is normally interested in the formation energy of an isolated defect. However, in the SC approximation the supercell and at the same time the defect is periodically repeated over the space (see figure 2.2). The SC method can be still considered to be accurate if the defects are not interacting with their periodic images. However, in the case of defects interacting over the SC boundaries the obtained formation energy no more describes the energy of an isolated defect, but the energy depends on the SC size converging to that of an isolated defect in the limit of an infinitely large SC. The situation is particularly severe in the case of charged defects in which case the defects are interacting with each other through the long-range Coulomb interaction and the problem cannot be overcome by just increasing the SC size.

4.3.1 Electrostatic finite-size effect correction for charged defects

In the case of SC calculations for charged defects a homogeneous neutralizing background charge must be introduced into the system to prevent the SC energy from diverging [71]. In the plane wave codes utilizing periodic boundary conditions this corresponds to omitting the divergent $\mathbf{G} = 0$ term when calculating the Hartree potential in the reciprocal space (*i. e.*

the third term in equation 4.3). Introducing a defect into a bulk SC gives rise to a constant shift in the electrostatic potential, which cannot be determined from SC calculations alone [70]. Thus when comparing energies of defect and bulk SCs the electrostatic potential of the defect SC must be aligned with the electrostatic potential of the bulk SC using the potential alignment constant C [70], see below. In practice the energy convergence problem in the case of charged defects could be solved by replacing the periodic Hartree energy of the defect charge density by its nonperiodic counterpart. However the problem is that the exact form of the defect charge density is unknown and the charge density has to be approximated. The first attempt to solve the problem was the estimation of the interaction energy by the Madelung energy of point charges embedded into a homogeneous neutralizing background charge [72], *i.e.*,

$$\Delta E = \frac{\alpha q^2}{2\epsilon L}, \tag{4.26}$$

where α is the Madelung constant of the structure, q the defect charge, ϵ the macroscopic dielectric constant and L is the lattice constant of the SC. Makov and Payne [73] added a further term scaling as L^{-3} and describing the quadrupole moment of the distribution of the extra defect charge q into Eq. (4.26). With these two terms the energy correction can be fitted to calculated SC energies and the energy of the isolated defect can be extrapolated to the limit $L \to \infty$.

Recently, Freysoldt *et al.* [9] introduced a method in which the energy correction term consists of two terms, E^{inter} and E^{intra}. The E^{inter} term takes into account the self-interaction of the sum of the defect charge density and background charge with the artificial periodic potential, *i.e.*,

$$E^{\text{inter}} = \frac{1}{2}\int_\Omega [q_d(\mathbf{r}) + n][\tilde{V}_{q/0}(\mathbf{r}) - V_{q/0}(\mathbf{r})]d\mathbf{r}, \tag{4.27}$$

where $q_d(\mathbf{r})$ is the defect charge distribution, n is the neutralizing background charge, Ω is the SC volume and $\tilde{V}_{q/0}, V_{q/0}$ are the periodic and non periodic defect potentials with respect to the neutral defect. The E^{intra} term removes the interaction between the background charge and the potential $V_{q/0}$

$$E^{\text{intra}} = \int_\Omega n V_{q/0} d\mathbf{r}. \tag{4.28}$$

The potentials $\tilde{V}_{q/0}, V_{q/0}$ are then divided into short- and long-range parts in the form $V_{q/0}(\mathbf{r}) = V_q^{lr}(\mathbf{r}) + V_{q/0}^{sr}(\mathbf{r})$, $\tilde{V}_{q/0}(\mathbf{r}) = \tilde{V}_q^{lr}(\mathbf{r}) + \tilde{V}_{q/0}^{sr}(\mathbf{r})$. The long-range potential $V_q^{lr}(\mathbf{r})$ is the macroscopically screened Coulomb potential and the potential $\tilde{V}_q^{lr}(\mathbf{r})$ is obtained from the $V_q^{lr}(\mathbf{r})$ potential using the discrete Fourier transform (assuming that the extra defect charge density is contained within the SC). The short-range potentials are approximated to be the same for the periodic and non-periodic potentials up to the potential alignment constant C

$$\tilde{V}^{sr}_{q/0}(\mathbf{r}) = V^{sr}_{q/0}(\mathbf{r}) + C. \tag{4.29}$$

By combining Eqs. (4.27) and (4.28) the energy correction term can be expressed in the form

$$\begin{aligned} \Delta E &= E^{\text{inter}} + E^{\text{intra}} \\ &= E^{\text{lat}}_q - q\Delta_{q/0}, \end{aligned} \tag{4.30}$$

where

$$E^{\text{lat}}_q = \int_\Omega \left[\frac{1}{2}[q_d(\mathbf{r}) + n][\tilde{V}^{\text{lr}}_q(\mathbf{r}) - V^{\text{lr}}_q(\mathbf{r})] + nV^{\text{lr}}_q(\mathbf{r}) \right] d\mathbf{r}, \tag{4.31}$$

$$\Delta_{q/0} = \frac{1}{\Omega} \int_\Omega V^{sr}_{q/0}(\mathbf{r}) d\mathbf{r}, \tag{4.32}$$

and

$$V^{sr}_{q/0}(\mathbf{r}) = \tilde{V}_{q/0}(\mathbf{r}) - \tilde{V}^{lr}_q(\mathbf{r}) - C. \tag{4.33}$$

Above, C is the potential alignment constant defined in Eq. (4.29). It is worth mentioning that the $\Delta_{q/0}$ term equals to $-C$ because the periodic potentials integrated over the periodic region equal to zero. The somewhat confusing point in the above derivation occurs in Eqs. (4.27) and (4.28). In equation (4.27) the term $nV_{q/0}(\mathbf{r})$ is taken into account by a factor one half, *i.e.*, the term is treated as a self-interaction term, while in equation (4.28) the term is taken into account as a whole, *i.e.* the background charge interacts with an external field, which seems to be a contradiction. Further, we were not able to reproduce the good convergence of the formation energy of the charged Ga vacancies with respect to SC size using Eq. (4.30) as was reported in Ref. [9]. In Ref. [10] the correction term was formulated in the form

$$\begin{aligned} \Delta E &= \int_\Omega \frac{1}{2} q_d(\mathbf{r}) \left(\tilde{V}^{lr}_q(\mathbf{r}) - V^{lr}_q(\mathbf{r}) \right) d\mathbf{r} + qC \\ &= \frac{2\pi}{\varepsilon\Omega} \sum_{\mathbf{G}\neq 0}^{|\mathbf{G}|\leq G_{cut}} \frac{q_d(|\mathbf{G}|)^2}{|\mathbf{G}|^2} - \frac{1}{\pi\varepsilon} \int_0^{G_{cut}} q_d(g)^2 dg + qC, \end{aligned} \tag{4.34}$$

where $q_d(g)$ is the model charge distribution in the reciprocal space and G_{cut} is an appropriately chosen cut-off radius ensuring the convergence of the correction term. In this form the correction term is a more flexible version of the Madelung correction (Eq. (4.26)). It is important to notice that Eq. (4.34) equals to Eq. (4.30) if the terms containing background charge n are omitted in Eq. (4.31). In this thesis the correction term is calculated using equation (4.34).

The intriguing property of the above method is that the potential alignment term and the validity of the approximation for the defect charge density can be visualized by comparing the calculated long range defect potential $\tilde{V}_q^{lr}(\mathbf{r})$ to that obtained from the SC calculations far from the defect. If the model charge density is appropriate the calculated $\tilde{V}_q^{lr}(\mathbf{r})$ should reproduce the potential $\tilde{V}_{defect} - \tilde{V}_{bulk}$ ($\tilde{V}_{defect}$ and $\tilde{V}_{bulk}$ are the defect and bulk SC electrostatic potentials), so that their difference forms far from the defect a constant plateau which equals to the potential alignment constant C. This is illustrated in figure 4.2. However, it is worth mentioning that if the point-like approximation for the defect charge distribution is not valid not much can be done.

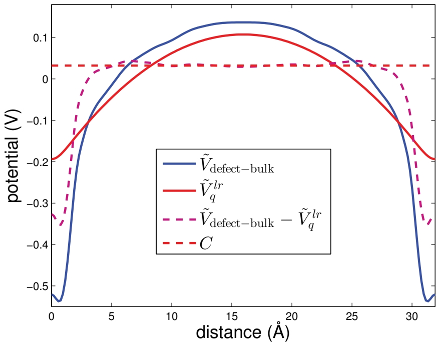

Figure 4.2. Different potential terms related to energy correction term in the case of gallium vacancy in GaAs in the -3 charge state. The potentials are averaged over the planes along the z-axis of the SC. The defect is located at the origin.

5. Nitrogen and Bi induced modifications in the electronic structures of GaAs, GaP and GaSb

5.1 Substitutional nitrogen in GaAs and GaSb

It is well known that replacing As atoms by just a small fraction of N atoms in GaAs leads to a significant decrease in the band gap as a function of N concentration [17]. In $\mathrm{GaSb}_{1-x}\mathrm{N}_x$ alloys the effect is even larger than in $\mathrm{GaAs}_{1-x}\mathrm{N}_x$ alloys [19]. The reason for the larger band gap reduction in $\mathrm{GaSb}_{1-x}\mathrm{N}_x$ is often suggested to be related to the larger electronegativity mismatch between the N and Sb atoms compared to that of the N and As atoms. Consequently, in the BAC model the interaction between the N resonant state and the host material CBE would then be stronger in the $\mathrm{GaSb}_{1-x}\mathrm{N}_x$ alloy. Although $\mathrm{GaSb}_{1-x}\mathrm{N}_x$ alloys have been modelled successfully using TB methods [74], DFT studies of this material are cumbersome because of the well known underestimation of the band gap when the (semi) local functionals are used. In the case of $\mathrm{GaSb}_{1-x}\mathrm{N}_x$ alloys the band gap completely closes when LDA is used and observing the N-induced band gap narrowing becomes unfeasible.

In Publication I we studied $\mathrm{GaAs}_{1-x}\mathrm{N}_x$ and $\mathrm{GaSb}_{1-x}\mathrm{N}_x$ alloys within the DFT formalism using the HSE06 hybrid functional. The HSE06 functional gives band gaps near to the experimental ones and enables the band structure calculations for $\mathrm{GaSb}_{1-x}\mathrm{N}_x$ alloys without any empirical parameter fitting. The main goal in Publication I was to study the modifications in the electronic structure of $\mathrm{GaSb}_{1-x}\mathrm{N}_x$ alloys and compare those to $\mathrm{GaAs}_{1-x}\mathrm{N}_x$ alloys. In addition, we studied the relative binding energies of different two-N-atom configurations in a SC. Besides configurations in which N atoms substitute Sb atoms we considered also the N_2 dimer on the Sb site.

The main conclusion in Publication I was that N affects the band structures of both GaAs and GaSb qualitatively and even quantitatively similarly. In both alloys N forms a localized state above the CBE resulting in a sharp peak in the LDOS at the N atom. The peak forms a long tail, having equal lengths in the two materials, extending into the band gap and causing the band gap narrowing. According to our calculations the most likely reason for the larger band gap reduction in $GaSb_{1-x}N_x$ compared to that in $GaAs_{1-x}N_x$ is the positions of the bulk CBEs with respect to the N induced resonant states in these alloys. In addition we found that in GaSb the formation of the N_2 dimers is energetically favorable. This may cause that notable amounts of nitrogen exist as N_2 dimers instead of substitutional nitrogen, which may lead to the poor quality of $GaSb_{1-x}N_x$ alloys for electronic applications.

5.2 N-N interactions in $GaAs_{1-x}N_x$ and $GaP_{1-x}N_x$ alloys and the band gap bowing

In Publication I it was observed that the band gap reduction in $GaAs_{1-x}N_x$ and $GaSb_{1-x}N_x$ alloys is caused by localized N states extending towards the band gap. Furthermore, it was observed that the band gap reduction in the case of multiple N atoms in the SC depends on the configuration of the substituted N atoms in accordance with the previous studies [13, 75]. These observations suggest that the N atoms are somehow coupled to each other, even if the actual mechanism for N-N interactions remained open in Publication I.

The work in Publication II was sparked by the observation that the CBE charge density in $GaAs_{1-x}N_x$ and $GaP_{1-x}N_x$ alloys is agglomerated along the zigzag chains originating from strong and relatively short Ga-N bonds and characterized by a strong intertwining of the electron structure and ion relaxation. This is illustrated in figure 5.1 which shows the CBE charge density in the case of a single N atom in the SC of 512-atoms in GaAs. In the figure, the twelve zigzag chains are directed along the twelve $\langle 110 \rangle$ directions. In Publication II it was also observed that the N-induced characteristic features in the electronic structures of these materials manifest themselves as localized peaks in the LDOSs at the N atom. These peaks were found to remain stationary with respect to the N concentration, but the broadenings of these peaks, occurring as long low intensity tails, increase and extend longer into the band gap leading to a stronger band gap reduction with the increasing N concentration. These observa-

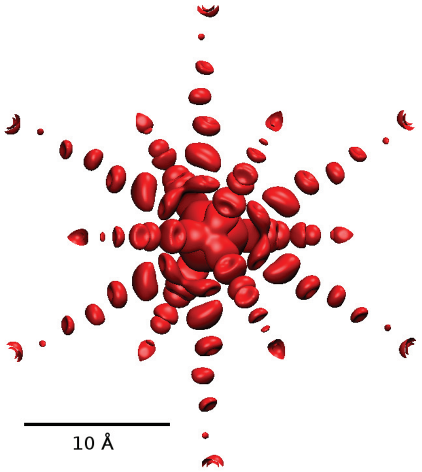

Figure 5.1. CBE partial charge density in the $Ga_{256}As_{255}N$ SC, viewed along the $\langle 111\rangle$ direction. The isosurface shown corresponds to a density isovalue of 0.0012.

tions are in a good agreement with the band broadening picture suggested by Deng *et al.* [76] indicating that the band gap narrowing is related to N-N interactions. Figure 5.2 indeed shows how the N atoms become coupled through the zigzag chains. Due to the periodic boundary conditions used in the SC-DFT calculations there is always another N atom standing on the same zigzag chain, as is shown in figure 5.2. Thus the N atoms become coupled to each other through these chains and with the increasing N concentration the distances between the N atoms become smaller leading to a stronger coupling and larger broadening of the N-related states as can be seen in the LDOSs in Publication II.

In Publication II the DFT calculations were limited to only a few N atoms in a SC under the periodic boundary conditions. To overcome this deficiency we developed a TB model based on our SC-DFT calculations. In the developed TB model the N atoms are allowed to interact with each other only along the $\langle 110\rangle$ directions and the matrix elements between N atoms i and j are defined as $h_{i,j} = k/r_{i,j}^{\alpha}$ if the N atoms i, j are connected through a zigzag chain and $h_{i,j} = 0$ otherwise. The calculation of the matrix elements in the SC approach and Γ-point approximation is discussed in more detail in Appendix A. The parameters k and α are obtained by fitting the produced eigenvalue distributions to the LDOSs of our SC-DFT calculations (see Publication II for details). The obtained parameters for $GaAs_{1-x}N_x$ are $k = -0.67$ eVÅ$^{\alpha}, \alpha = 1.28$ and for $GaP_{1-x}N_x$ $k = -0.59$ eVÅ$^{\alpha}, \alpha = 1.43$. The small values of α for both materials indicates that the N atoms are coupled to each other through a long-range interaction.

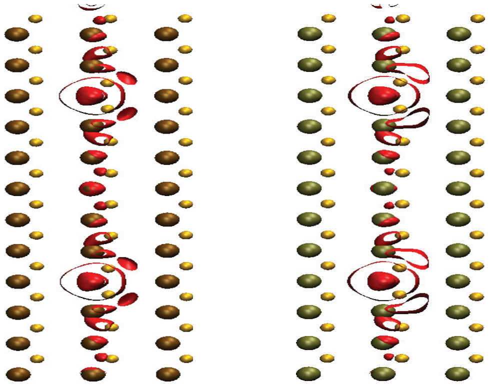
(a) $\mu = 0.002$ **(b)** $\mu = 0.002$

Figure 5.2. (Color online) Partial charge-densities in the (110) planes corresponding to CBE in $Ga_{108}As_{107}N$ (a) and $Ga_{108}P_{107}N$ (b) SCs. The yellow spheres corresponds to Ga atoms, the brown spheres to As atoms and the tan spheres to P atoms. N atoms are located inside the centers of high charge accumulation. The μ-value indicates the isovalue used.

This is possible due to a directional, effectively 1-d interaction preventing the total energy from diverging. The developed TB model takes only into account the interactions between the N atoms. With this model we are able to simulate tens of thousands of N atoms randomly distributed in the host material in accordance with the experimental conditions. Within the developed model we obtain eigenvalue distributions corresponding to the broadening of the N induced states which can be compared to experimental measurements.

In Ref. [77] Ivanova *et al.* measured scanning tunneling spectra of $GaAs_{1-x}N_x$ alloys and observed characteristic features in the spectra corresponding to an isolated N atom and to nearest neighbor N-N atom pairs. These features are also present in our calculated eigenvalue distributions as shown in figure 5.3 in the case of 3.1% N concentration in the $GaAs_{1-x}N_x$ alloy. In figure 5.3 the two side peaks are due to the nearest neighbor N-N pairs and the peak in the middle corresponds to the isolated nitrogen.

In experiments the often measured key quantities in $GaAs_{1-x}N_x$ and $GaP_{1-x}N_x$ alloys are the E_- and E_+ states as a function of the N concentration (see section 2.1.1). In our model these states correspond to the minimum and maximum eigenvalues of the calculated eigenvalue distributions (see figure 5.3). It is important to notice that our model produces a continuous distribution of eigenvalues between the extreme eigenvalues corresponding to the broadening of the N-induced states. In Publication

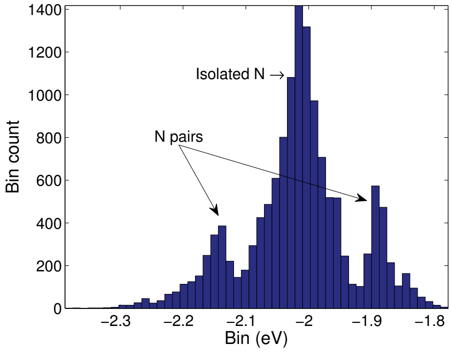

Figure 5.3. TB eigenvalue distribution corresponding to a random sample of 13,824 N atoms (3.1% concentration) in the GaAs$_{1-x}$N$_x$ alloy.

II we randomly distributed different numbers of N atoms into a large SC and solved these systems using the developed TB method. At each concentration the minimum and maximum eigenvalues were recorded and averaged over 100 samples. In this way we obtained the E_- and E_+ states as a function of the N concentration.

In the case of GaAs$_{1-x}$N$_x$ and GaP$_{1-x}$N$_x$ alloys the E_- and E_+ states are directly measured in experiments allowing a direct comparison to our calculated E_- and E_+ states. This is done in figure 5.4. In addition the results calculated by the SC-DFT scheme are shown. In Publication II the calculated E_- and E_+ states, shown in figure 5.4, are found to be in a good qualitative and quantitative agreement with the experimental results. The calculated E_- and E_+ states show the typical square-root-like behavior as a function of the N concentration in the case of random structures while the SC-DFT calculated E_- state shows a linear dependence. The wrong concentration dependence of the band gap reduction in SC-DFT calculations [13, 30] can be well explained by the directional interaction between the N atoms. Due to the periodic boundary conditions the N atoms of the neighboring SCs are always located on a common zigzag chain leading to a surplus of N-N interactions compared to random distributions.

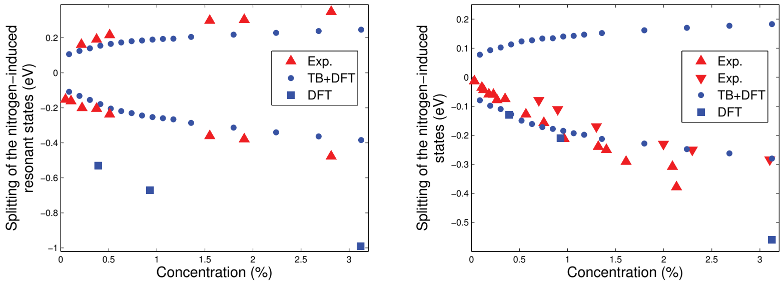

(a) **(b)**

Figure 5.4. Experimental and calculated E_- and E_+ states as a function of N concentration in (a) $GaAs_{1-x}N_x$ and (b) $GaP_{1-x}N_x$. The blue circles and squares give the calculated random-system TB and the SC-DFT results, respectively. The red triangles are the experimental data for $GaAs_{1-x}N_x$ (data is from Ref. [25] (measurement temperature 300 K)) and $GaP_{1-x}N_x$ (red upright triangles are from Ref. [20] (20 K) and red downright triangles are from Ref. [26] (room temperature)).

5.3 Bi induced modifications in the electronic structures of $GaAs_{1-x}Bi_x$ alloys

After the observation in Publication II that the band gap narrowing in $GaAs_{1-x}N_x$ and $GaAs_{1-x}P_x$ alloys is connected to the broadening of the N induced states due to N-N interactions, a natural next step was to study if the same mechanism is also valid in $GaAs_{1-x}Bi_x$ alloys. Despite the large number of computational studies considering $GaAs_{1-x}Bi_x$ alloys only a few *ab initio* studies with the band structure and DOS calculations can be found. Thus the location of Bi states within the valence band as well as the anomalously large SO splitting are still puzzling problems in this alloy. In Publication III we studied Bi-induced modifications in the electronic structure of GaAs. In this work we used the DFT framework within LDA. The SO coupling was included in all calculations.

In Publication III we observed a similar localized peak near the VBE which broadens with the increasing Bi concentration as was observed in Publication II in the conduction band of $GaAs_{1-x}N_x$ alloys. However the band structures, figures 5.5(a), 5.5(b) and 5.5(c), show different characteristics compared to band structures of $GaAs_{1-x}N_x$ alloys in Publication II. In $GaAs_{1-x}N_x$, substitutional N atoms form a flat impurity-like band of s-character corresponding to the localized peak observed in the LDOSs at the N atoms. However, in the case of $GaAs_{1-x}Bi_x$ a similar impurity-like band corresponding to the localized peak near the VBE cannot be seen. This is in agreement with the suggestion by Zhang *et al.* [38] that no new

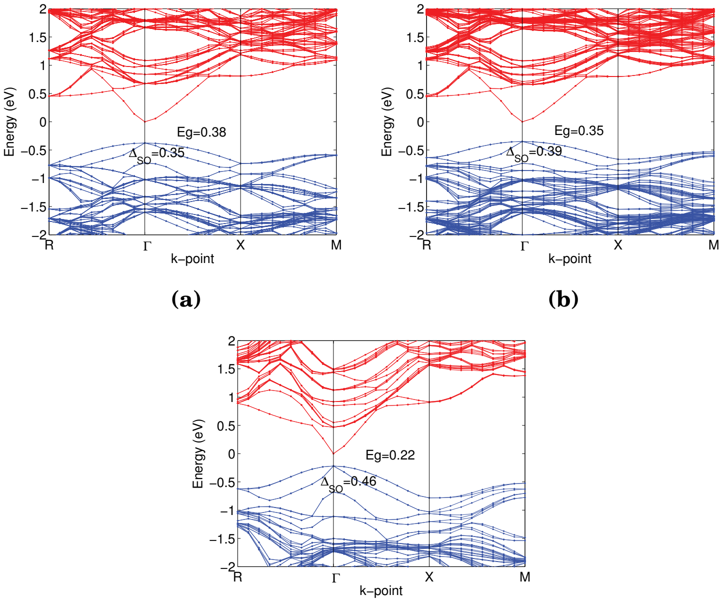

(a) **(b)**

(c)

Figure 5.5. (Color online) Band structures for bulk $Ga_{108}As_{108}$ (a), $Ga_{108}As_{107}Bi$ (b) and $Ga_{32}As_{31}Bi$ (c). The energy zero coincide with the conduction band minimum (CBM). The vertical lines are guide to an eye and indicate the positions of the high-symmetry points.

states are added to the valence band and the Bi states could be interpreted as strongly perturbed host states.

Despite the differences in the band structures of $GaAs_{1-x}Bi_x$ alloys compared to $GaAs_{1-x}N_x$ alloys, the VBE charge density in $GaAs_{1-x}Bi_x$ alloys was found to resemble the CBE charge density in $GaAs_{1-x}N_x$ alloys in Publication II, *i.e.*, the VBE in $GaAs_{1-x}Bi_x$ alloys becomes agglomerated along the zigzag chains originating from the Bi atoms. This leads to interactions between the Bi atoms and to the broadening of the mixed Bi-bulk states near the alloy VBE in analogous to the broadening of the N-induced states in $GaAs_{1-x}N_x$ alloys. The broadening of the mixed Bi-bulk states then leads to a broadening of the alloy VBE resulting in the band gap narrowing. In Publication III we modelled the broadening of the mixed Bi-bulk states using the same TB model as in Publication II. However, in the case of $GaAs_{1-x}Bi_x$ alloys we cannot directly compare the calculated E_- and E_+ states to experiments, as in the case of $GaAs_{1-x}N_x$ alloys, because in experiments only the band gap at different Bi concentrations is measured instead of E_- and E_+ states. Thus in Publication III we calculated the band gap reduction at different Bi concentrations in the case of

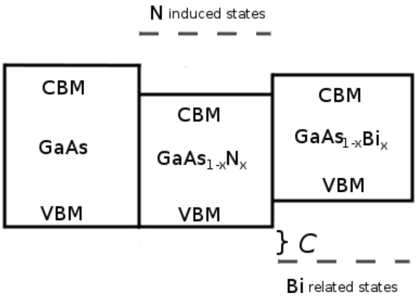

Figure 5.6. Relative positions of the CBM and VBM in bulk GaAs, GaAs$_{1-x}$N$_x$ and GaP$_{1-x}$N$_x$. The distance C indicates the distance between the mixed Bi-bulk state near the alloy VBE and the bulk VBM.

randomly distributed Bi atoms using the equation

$$\Delta E_g(x) = -\max\{s(x) - C, 0\} - bx. \tag{5.1}$$

Above, x stands for the Bi concentration, b is the CBM downwards shift per percent originating from the Vegard's law, $s(x)$ is the splitting of the peak corresponding to the mixed Bi-bulk states near the alloy VBE in the random structures and C is the distance of the peak corresponding to the mixed Bi-bulk states near the alloy VBE from the bulk VBM (see figure 5.6).

In Publication III the calculated band gap behavior was found to be in a qualitative and quantitative agreement with the experimental one. However, it was also observed that the strict location of the mixed Bi-bulk states in the valence band is a function of the Bi concentration decreasing with the increasing Bi concentration. The dependence of the calculated Bi states on the Bi concentration was also observed in Refs. [37, 38]. In Publication III the location of the mixed Bi-bulk states was approximated to be constant which creates some uncertainty to the predictive power of the applied TB model. One of the main conclusions in Publication III was that the anomalously large SO splitting energy can be explained to result from the VBE broadening due to the Bi-Bi interactions. This conclusion is in agreement with the photomodulated spectroscopy measurements of Kudrawiec *et al.* [35] which show that the $E_0 + \Delta_{SO}$ transition is rather insensitive to the addition of 3% Bi, indicating that the increase of the SO splitting is due to the rising VBE.

6. Hybrid functional study of native point defect energetics in GaSb

GaSb is an interesting material from both material and device point of views. It can be used as a substrate material for other III-V compounds covering a wide spectral range from 0.8 to 4.3 μm [78]. The electronic properties of GaSb can be also significantly modified by substituting a small fraction of Sb by N [19, 79], which was also observed in our own calculations in Publication I. Undoped GaSb is always p-type and the p-type conductivity is often connected to native point defects, *e.g.*, Ga vacancies and antisites [78]. However, the origin of the p-type conductivity is still debated. In GaSb also a strongly asymmetric self-diffusion, in which Ga atoms diffuse over three orders of magnitude faster than Sb atoms, has been reported [80]. The strongly asymmetric self-diffusion is explained by atoms diffusing in their own sublattices via vacancies [80] or as interstitials [81].

In Publication IV we studied the native point defect energetics in GaSb within the DFT framework using the HSE06 hybrid functional. The formation energies were computed using Eq. (4.25) and for charged defects the energy correction term was calculated using Eq. (4.34). Due to the HSE06 hybrid-functional we were able to overcome the significant underestimation of the GaSb band gap when LDA is used. In GaSb the chemical potentials, occurring in Eq. (4.25), are obtained as follows. In Ga (Sb)-rich growth conditions μ_{Ga} (μ_{Sb}) equals to that of $\mu_{\mathrm{Ga[bulk]}}$ ($\mu_{\mathrm{Sb[bulk]}}$) and in Sb (Ga) -rich growth conditions μ_{Ga} (μ_{Sb}) is obtained as $\mu_{\mathrm{Ga}} = \mu_{\mathrm{GaSb}} - \mu_{\mathrm{Sb[bulk]}}$ ($\mu_{\mathrm{Sb}} = \mu_{\mathrm{GaSb}} - \mu_{\mathrm{Ga[bulk]}}$), where μ_{GaSb} is the energy of the two-atom unit of bulk GaSb [70]. The chemical potentials for bulk Ga and Sb are calculated in their point symmetries Cmca and $\mathsf{R\bar{3}m}$, respectively.

In Publication IV the use of the HSE06 hybrid functional was found to significantly affect the defect formation energies. The HSE06 hybrid functional clearly increases the formation energies compared to the lo-

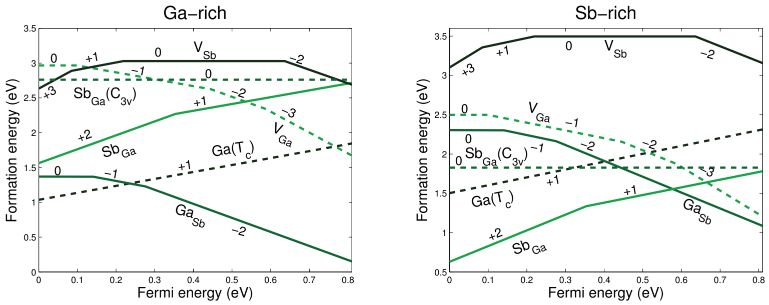

(a) **(b)**

Figure 6.1. Formation energies for stable charge states of point defects in GaSb as a function of the Fermi level in the Ga-rich (a) and Sb-rich (b) growth conditions.

cal functionals and qualitatively seems to favor the more positive charge states. The lowest-energy defects were found to be the Ga antisite, Ga interstitials and the Sb antisite. Figures 6.1(a) and 6.1(b) show the formation energies for different defects as a function of the Fermi level in the Ga-rich and Sb-rich growth conditions, respectively. The most prominent candidate for the source of p-type conductivity was found to be the $\mathrm{Ga}_{\mathrm{Sb}}^{2-}$, $\mathrm{Ga}_{\mathrm{Sb}}^{1-}$ antisites. However, in a strong contrast to a previous DFT study [81], where LDA was used, also the energies of the $\mathrm{Sb}_{\mathrm{Ga}}^{2+}$, $\mathrm{Sb}_{\mathrm{Ga}}^{1+}$ antisites were found to be significantly low in the Sb-rich growth conditions.

In the Sb-rich growth conditions the donor-like Sb antisites would turn the substrate into n-type or at least compensate the p-type conductivity, which is not observed in experiments. In Publication IV we suggested, based on our climbing-image nudged elastic band method calculations [82], the possibility that the positively-charged $\mathrm{Sb}_{\mathrm{Ga}}$ transforms into a neutral C_{3v} state to explain the absence of donor-like Sb antisites in experiments. We also studied the carbon and oxygen impurities, which are common acceptors in AlSb [83]. We found that especially the interstitial, acceptor-like, oxygen has a notably low formation energy and could also compensate for the electrical activity of the $\mathrm{Sb}_{\mathrm{Ga}}$ antisite.

7. Conclusions

7.1 Developed theory to describe electronic structures of III-V-N alloy semiconductors

In this dissertation an alternative quantum mechanical theory to describe N-induced modifications in electronic structures of III-V compound semiconductors was developed and further extended to Bi alloying of these materials. In the developed theory the band gap narrowing in III-V-N alloys originates solely from N-N interactions and the host material atoms only mediate the interaction. The developed method is in a contrast to the currently most widely accepted band anticrossing (BAC) model, in which the band gap narrowing results from the interaction between the N-induced states and the host material conduction band edge (CBE). The great advantage of the developed theory is that it can be mathematically described using the developed tight binding (TB) model, which rely purely on *ab initio* methods and there is no need for any external fitted parameters. The developed TB model allows simulation of huge random structures and a direct comparison between the theory and experiments, *e.g.*, the measured scanning tunneling spectra [77] can be compared to the calculated energy distributions. In the developed TB model the occurrence of the E_- and E_+ states are a natural consequence of the N-N interactions and the model correctly predicts their behavior as a function of the N concentration. Further, the model explains in a natural way the difference between the simulations performed for ordered structures compared to those for random structures. These are clear improvements over the BAC model in which the band gap as a function of the N concentration must be first either experimentally measured or simulated in random structures to obtain the needed parameters of the model for the mechanism of the band gap narrowing.

The essential feature in the developed theory is that the CBE becomes strongly agglomerated along the zigzag chains in the $\langle 110 \rangle$ directions and loses its bulk character with the increasing N concentration. The directional interaction is due to a strong intertwining of the electronic structure and ionic relaxation. This feature should be studied in a future work in more detail as a possible solution to the observed poor electron mobility in these alloys. Further, according to the developed model the alloy loses its strict band structure and the energy bands become distributed over a wide energy range. This is in accordance with the effective band structure model in random alloys by Popescu *et al.* in Ref. [84].

7.2 Generalization of the developed model to $\mathbf{GaAs}_{1-x}\mathbf{Bi}_x$ alloys

In Publication III the developed model to describe the N-induced modifications of $\mathrm{GaAs}_{1-x}\mathrm{N}_x$ alloys was successfully generalized to $\mathrm{GaAs}_{1-x}\mathrm{Bi}_x$ alloys in which the electronic structure modifications occurs in the valence band. Our calculations confirm the previous assumption by Zhang *et al.* [38] that Bi does not induce clear impurity-like states in $\mathrm{GaAs}_{1-x}\mathrm{Bi}_x$ alloys, but instead, the Bi states are strongly mixed with the bulk states. In Publication III we showed that the band gap narrowing is a result of the broadening of these mixed Bi-bulk states due to the Bi-Bi interactions. One of the main conclusions in the case of $\mathrm{GaAs}_{1-x}\mathrm{Bi}_x$ alloys was that the experimentally observed anomalously large spin-orbit (SO) splitting energy is a natural consequence of the valence band edge (VBE) broadening. This conclusion may hinder some of the expectations for this material in spintronic applications. However, the possibility for the damping of the Auger recombination process from the VBE into the SO-split-off band should not be affected, although it may be not so dominating as in the case of a sharp bandstructure of an ordered solid.

7.3 Native point-defect energetics in GaSb and the connection to p-type conductivity

In Publication IV the native point-defect energetics was extensively studied in GaSb to explain the growth-condition independent p-type conductivity. In contrast to earlier computational studies related to GaSb we used a hybrid functional in our density functional theory (DFT) calculations instead of the local density approximation (LDA). Importantly, the more accurate exchange-correlation-energy functional was found to affect not only the band gap but also qualitatively and quantitatively the calculated formation energies. Even though our calculations supported the p-type conductivity in the Ga-rich growth conditions the results did not give direct support for the p-type conductivity in the Sb-rich growth conditions because of the predicted abundance of donor-like $\mathrm{Sb}_{\mathrm{Ga}}$ antisites. To explain the p-type conductivity in the Sb-rich growth conditions we studied using the climbing-image nudged elastic band method the possibility that the donor-like $\mathrm{Sb}_{\mathrm{Ga}}$ antisites transform into metastable neutral $C_{3\mathrm{v}}$ configurations. Our calculations revealed that the neutral C_{3v} configuration is located at the same level in energy as the T_d configuration separated by a relatively small barrier. This would allow effective thermal excitations from the neutral T_d configuration into the C_{3v} configuration after capturing the excess electrons into a strong and narrow resonance above the CBE. However, it is not clear what could prevent the electrons to be excited and the relaxation back to the T_d configuration. To confirm or reject our hypothesis would require accurate experimental measurements for the energetics of different defects, which are not currently available.

A. Calculation of the matrix elements in the developed tight-binding method

In the developed TB model the non-diagonal matrix elements $h_{i,j}$, describing the interaction between nitrogen atoms at sites i and j, are defined as $h_{i,j} = k/r_{i,j}^{\alpha}$ if the atoms i and j are connected trough a zig-zag chain (the linear chains in the twelve $\langle 110 \rangle$ directions) and $h_{i,j} = 0$ otherwise. The diagonal terms $h_{i,i}$ are set to an arbitrary chosen constant value E_{s^*} which describes the energy of the isolated N-induced states.

In the SC approximation with periodic boundary conditions and the Γ-point approximation the non-zero matrix elements $h_{i,j}$ (without restriction of the interaction to the zigzag chains) have the form

$$h_{i,j} = \sum_{\mathbf{L}} \frac{k}{|\hat{\mathbf{r}}_{i,j} + \mathbf{L}|^{\alpha}}, \tag{1.1}$$

where $\hat{\mathbf{r}}_{i,j}$ is the connecting vector between N atoms at sites i and j at the SC and $\mathbf{L}$ is the SC lattice vector. The units are in electron volts and

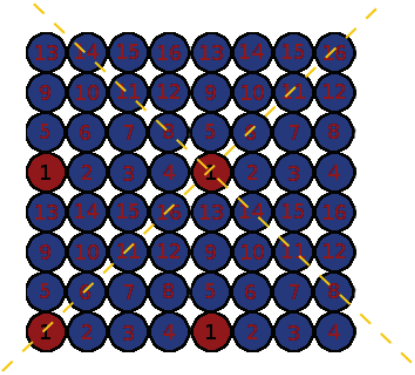

Figure 1.1. Illustration of the procedure determining whether the N atoms i and j are connected by a zigzag chain or not. The figure shows the situation in which the SC contains 16 atoms, labelled 1,2,...,16 and the row element in question is 1. If the row element would have some other index i the atom i should be first translated at the origin, *i.e.*, at the position of the atom 1 in the figure. The yellow dashed lines indicate that atoms 6,8,11,14, and 16 are connected by a zigzag chain to atom 1. The atom 11 is connected in four octants of space whereas the others are connected in two octants.

angstroms. To determine if a N atom i is connected to a N atom j or its periodic replicas the SC is translated so that the atom i (the row element) is at the origin of the SC. Then dot products between the normalized connecting vector $\hat{\mathrm{r}}_{i,j}/|\hat{\mathrm{r}}_{i,j}|$ and the normalized direction vectors $\langle 110\rangle/\sqrt{2}$ are taken. Here, $\langle 110\rangle$ indicates any of the directions $\hat{\imath}+\hat{\jmath}, \hat{\imath}-\hat{\jmath}, ..., \hat{\jmath}+\hat{k}$. If any of the dot products is 1 or -1 then the atoms i and j are connected by a zigzag chain. The above procedure must be repeated for N atoms j in every octant of the three-dimensional space, labeled by ϕ below. In practice this is done by periodically translating the N atoms j into every octant. If the atom i is connected to the atom j in a particular octant it is also connected to all periodic replicas of the atom j in that direction separated by the distance $\sqrt{2}L$. This is illustrated in two dimensions in figure 1.1.

The restriction of the interactions to the interconnecting zig-zag chains modifies Eq. (1.1) so that in the case of simple-cubic SCs it becomes

$$h_{i,j} = \sum_{\phi}\sum_{n=0}^{\infty} \frac{k}{\left(r_{i,j_\phi} + \sqrt{2}nL\right)^{\alpha}}, \tag{1.2}$$

where ϕ runs over all the octants in which the N atoms i and j are connected and L is the lattice parameter. The diagonal term reads as

$$h_{i,i} = E_{s^*} + 12\sum_{n=1}^{\infty} \frac{k}{\left(\sqrt{2}nL\right)^{\alpha}}. \tag{1.3}$$

The inner sum in Eq. (1.2) is the Hurwitz zeta function and it can be evaluated efficiently using the Euler-Maclaurin summation formula [85]. The Euler-Maclaurin summation was originally used to approximate definite integrals. However, it can be also used to approximate finite and even infinite sums of the form

$$\begin{aligned}\sum_{n=a}^{b} f(n) \quad &\sim \quad \int_a^b f(x)dx + \frac{f(a)+f(b)}{2} \\ &+\sum_{k=1}^{\infty} \frac{B_{2k}}{(2k)!}\left(f^{(2k-1)}(b) - f^{(2k-1)}(a)\right),\end{aligned} \tag{1.4}$$

where B_k is the k:th Bernoulli number and f^k is the k:th derivative of the function f. In the case of Hurwitz zeta function the function f is

$$f(s,q) = \frac{1}{(q+n)^s} \tag{1.5}$$

and the k:th derivative is easily calculated obtaining

$$f^k(s,q) = \left(\prod_{i=0}^{k-1}(-s-i)\right)\frac{1}{(q+n)^{s-k}}, \tag{1.6}$$

where Π is the product symbol.

Bibliography

[1] J. Singh, *Semiconductor Optoelectronics: Physics and Technology*, McGraw-Hill, New York (1995)

[2] J. S. Harris Jr, "GaInAs long-wavelength lasers: progress and challenges", Semiconductor Science and Technology, **17**, 880 (2002)

[3] N. Lopeź, L. A. Reichertz, K. M. Yu, K. Campman, W. Walukiewicz, "Engineering the Electronic Band Structure for Multiband Solar Cells", Physical Review Letters, **106**, 028701 (2011)

[4] G. Wolfowicz, A. M. Tyryshkin, R. E. George, H. Riemann, N. V. Abrosimov, P. Becker, H.-J. Pohl, M. L. W. Thewalt, S. A. Lyon, J. L. Morton, "Atomic clock transitions in silicon-based spin qubits", Nature Nanotechnology, **8**, 561 (2013)

[5] A. Morello, J. J. Pla, F. A. Zwanenburg, K. W. Chan, K. Y. Tan, H. Huebl, M. Möttonen, C. D. Nugroho, C. Yang, J. A. van Donkelaar, A. D. C. Alves, D. N. Jamieson, C. C. Escott, L. C. L. Hollenberg, R. G. Clark, A. S. Dzurak, "Single-shot readout of an electron spin in silicon", Nature, **467**, 687 (2010)

[6] F. Schwabl, *Quantum Mechanics*, Springer, Berlin, 3rd ed. (2002)

[7] P. Hohenberg, W. Kohn, "Inhomogeneous Electron Gas", Physical Review, **136**, B864 (1964)

[8] W. Kohn, L. J. Sham, "Self-Consistent Equations Including Exchange and Correlation Effects", Physical Review, **140**, A1133 (1965)

[9] C. Freysoldt, J. Neugebauer, C. G. Van de Walle, "Fully *Ab Initio* Finite-Size Corrections for Charged-Defect Supercell Calculations", Physical Review Letters, **102**, 016402 (2009)

[10] C. Freysoldt, J. Neugebauer, C. G. Van de Walle, "Electrostatic interactions between charged defects in supercells", Physica status solidi B, **248**, 1067 (2010)

[11] S. M. Sze, *Semiconductor devices: Physics and Technology*, John Wiley and Sons, New York (1985)

[12] A. Kokalj, "Computer graphics and graphical user interfaces as tools in simulations of matter at the atomic scale", Computational Materials Science, **22**, 155 (2003)

[13] P. R. C. Kent, A. Zunger, “Theory of electronic structure evolution in GaAsN and GaPN alloys”, Physical Review B, **64**, 115208 (2001)

[14] Y. Zhang, A. Mascarenhas, J. F. Geisz, H. P. Xin, C. W. Tu, “Discrete and continuous spectrum of nitrogen-induced bound states in heavily doped $GaAs_{1-x}N_x$”, Physical Review B, **63**, 085205 (2001)

[15] D. G. Thomas, J. J. Hopfield, C. J. Frosch, “Isoelectronic Traps Due to Nitrogen in Gallium Phosphide”, Physical Review Letters, **15**, 857 (1965)

[16] X. Liu, M.-E. Pistol, L. Samuelson, S. Schwetlick, W. Seifert, “Nitrogen pair luminescence in GaAs”, Applied Physics Letters, **56**, 1451 (1990)

[17] M. Weyers, M. Sato, H. Ando, “Red Shift of Photoluminescence and Absorbtion in Dilute GaAsN Alloy Layers”, Japanese Journal of Applied Physics, **31**, 853 (1992)

[18] J. F. Geisz, D. J. Friedman, “III-N-V semiconductors for solar photovoltaic applications”, Semiconductor Science Technology, **17**, 769 (2002)

[19] T. D. Veal, L. F. J. Piper, S. Jollands, B. R. Bennet, P. H. Jefferson, P. A. Thomas, C. F. McConville, B. N. Murdin, L. Buckle, G. W. Smith, T. Ashley, “Band gap Reduction in GaNSb alloys due to the anion mismatch”, Applied physics Letters, **87**, 132101 (2005)

[20] H. Yaguchi, S. Miyoshi, G. Biwa, M. Kibune, K. Onabe, Y. Shiraki, R. Ito, “Photoluminescence excitation spectroscopy of $GaP_{1-x}N_x$ alloys: conduction-band-edge formation by nitrogen incorporation”, Journal of Crystal Growth, **170**, 353 (1997)

[21] W. Shan, W. Walukiewicz, J. W. Ager III, E. E. Haller, J. F. Geisz, D. J. Friedman, J. M. Olson, S. R. Kurtz, “Band Anticrossing in GaInAs Alloys”, Physical Review Letters, **82**, 1221 (1999)

[22] P. R. C. Kent, L. Bellaiche, A. Zunger, “Pseudopotential theory of dilute III-V nitrides”, Semiconductor Science Technology, **17**, 851 (2002)

[23] D. L. Young, J. F. Geisz, T. J. Coutts, “Nitrogen-induced decrease of the electron effective mass in $GaAs_{1-x}N_x$ thin films measured by thermomagnetic transport phenomena”, Applied Physics Letters, **82**, 1236 (2003)

[24] M. Reason, Y. Jin, H. A. McKay, N. Mangan, D. Mao, R. S. Goldman, X. Bai, C. Kurdak, “Influence of N on the electronic properties of GaAsN alloy films and heterostructures”, Journal of Applied Physics, **102**, 103710 (2007)

[25] P. J. Klar, H. Grüning, W. Heimbrodt, J. Koch, F. Höhnsdorf, W. Stolz, P. M. A. Vicente, J. Camassel, “From N isoelectronic impurities to N-induced bands in the GaN_xAs_{1-x} alloy”, Applied Physics Letters, **76**, 3439 (2000)

[26] W. Shan, W. Walukiewicz, K. M. Yu, J. Wu, J. W. Ager, E. E. Haller, H. P. Xin, C. W. Tu, “Nature of the fundamental band gap in GaN_xP_{1-x} alloys”, Applied Physics Letters, **76**, 3251 (2000)

[27] W. Walukiewicz, W. Shan, K. M. Yu, J. W. Ager III, E. E. Haller, I. Miotkowski, M. J. Seong, H. Alawadhi, A. K. Ramdas, “Interaction of Localized Electronic States with the Conduction Band: Band Anticrossoing in II-VI Semiconductor Ternaries”, Physical Review Letters, **85**, 1552 (2000)

[28] P. W. Anderson, “Localized Magnetic States in Metals”, Physical Review, **124**, 41 (1961)

[29] C. Harris, A. Lindsay, E. P. O’Reilly, “Evolution of N defect states and optical transition in ordered and disordered $\mathrm{GaP}_{1-x}\mathrm{N}_x$ alloys”, Journal of Physics: Condensed Matter, **20**, 295211 (2008)

[30] V. Virkkala, V. Havu, F. Tuomisto, M. J. Puska, “Hybrid functional study of band structures of $\mathrm{GaAs}_{1-x}\mathrm{N}_x$ and $\mathrm{GaSb}_{1-x}\mathrm{N}_x$ alloys”, Physical Review B, **85**, 085134 (2012)

[31] R. N. Kini, L. Bhusal, A. J. Ptak, R. France, A. Mascarenhas, “Electron Hall mobility in GaAsBi”, Journal of Applied Physics, **106**, 043705 (2009)

[32] A. Janotti, S.-H. Wei, S. B. Zhang, “Theoretical study of the effects of isovalent coalloying of Bi and N in GaAs”, Physical Review B, **65**, 115203 (2002)

[33] B. Fluegel, S. Francoeur, A. Mascarenhas, S. Tixier, E. C. Young, T. Tiedje, “Giant Spin-Orbit Bowing in $\mathrm{GaAs}_{1-x}\mathrm{Bi}_x$”, Physical Review Letters, **97**, 067205 (2006)

[34] S. J. Sweeney, Z. Batool, K. Hild, S. R. Jin, T. J. C. Hosea, “The Potential Role of Bismide Alloys in Future Photonic Devices”, 1–4, 13th International Conference on Transparent Optical Networks (ICTON), IEEE, Stockholm (2011)

[35] R. Kudrawiec, J. Kopaczek, P. Sitarek, J. Misiewicz, M. Henini, S. V. Novikov, “Unusual broadening of E_0 and $E_0 + \Delta_{SO}$ transitions in GaAsBi studied by electromodulation spectroscopy”, Journal of Applied Physics, **111**, 066103 (2012)

[36] K. Alberi, J. Wu, W. Walukiewicz, K. M. Yu, O. D. Dubon, S. P. Watking, C. X. Wang, X. Liu, Y.-J. Cho, J. Furdyna, “Valence-band anticrossing in mismatched III-V semiconductor alloys”, Physical Review B, **75**, 045203 (2007)

[37] M. Usman, C. A. Broderick, A. Lindsay, E. P. O. O’Reilly, “Tight-binding analysis of the electronic structure of dilute bismide alloys of GaP and GaAs”, Physical Review B, **84**, 245202 (2011)

[38] Y. Zhang, A. Mascarenhas, L.-W. Wang, “Similar and dissimilar aspects of III-V semiconductors containing Bi versus N”, Physical Review B, **71**, 155201 (2005)

[39] S. Elliot, *The Physics and Chemistry of Solids*, Wiley, Chippenham, Wiltshire (2006)

[40] M. C. Payne, M. P. Teter, D. C. Allan, T. A. Arias, J. D. Joannopoulos, “Iterative minimization techniques for *ab initio* total-energy calculations”, Reviews of Modern Physics, **64**, 1045 (1992)

[41] A. Luque, S. Hegedus, *Handbook of photovoltaic science and engineering*, John Wiley and Sons, Chichester, West Sussex, England (2003)

[42] W. Shockley, H. J. Queisser, “Detailed Balance Limit of Efficiency of $p-n$ Junction Solar Cells”, Journal of Applied Physics, **32**, 510 (1961)

[43] R. M. Swanson, “Approaching the 29% limit efficiency of silicon solar cells”, 889–894, Photovoltaic Specialists Conference, 2005. Conference Record of the Thirty-first IEEE, IEEE (2005)

[44] A. De Vos, “Detailed balance limit of efficiency of tandem solar cells”, Journal of physics D, **13**, 839 (1980)

[45] S. R. Kurtz, D. Myers, J. M. Olson, “Projected Performance of Three- and Four-Junction Devices Using GaAs and GaInP”, 1–4, 26th IEEE Photovoltaic Specialists Conference, IEEE, Anaheim, California (1997)

[46] F. Dimroth, “World Record Solar Cell with 44.7 % Efficiency”, `http://www.ise.fraunhofer.de/en/press-and-media/press-releases/presseinformationen-2013/world-record-solar-cell-with-44.7-efficiency` (2013)

[47] P. S. Zory, *Quantum well lasers*, Academic Press Inc., London (1993)

[48] C. A. Broderick, M. Usman, S. J. Sweeney, E. P. O. O’Reilly, “Band engineering in dilute nitride and bismide semiconductor lasers”, Semiconductor Science and Technology, **27**, 094011 (2012)

[49] M. Kondow, T. Kitatani, S. Nakatsuka, M. C. Larson, K. Nakahara, Y. Yazawa, M. Okai, “GaInNAs: A Novel Material for Long-Wavelength Semiconductor Lasers”, IEEE Journal of selected topics in quantum electronics, **3**, 719 (1997)

[50] G. Steinle, F. Mederer, M. Kicherer, R. Michalzik, G. Kristen, A. Y. Egorov, H. Riechert, H. D. Wolf, K. J. Ebeling, “Data transmission up to 10 Gbit/s with 1.34 μm wavelength InGaAsN VCSELs”, Electronic Letters, **37**, 632 (2001)

[51] R. M. Martin, *Electronic Structure: Basic Theory and Practical Methods*, CAMBRIDGE UNIVERSITY PRESS, Cambridge (2004)

[52] C. Møller, M. S. Plesset, “Note on an Approximation Treatment for Many-Electron Systems”, Physical Review, **46**, 618 (1934)

[53] G. Kresse, D. Joubert, “From ultrasoft pseudopotentials to the projector augmented-wave method”, Physical Review B, **59**, 1758 (1999)

[54] G. Kresse, J. Furthmüller, “Efficiency of ab-initio total energy calculations for metals and semiconductors using a plane-wave basis set”, Computational Materials Science, **6**, 15 (1996)

[55] K. Baarman, J. VandeVondele, “A comparison of accelerators for direct energy minimization in electronic structure calculations”, The Journal of Chemical Physics, **134**, 244104 (2011)

[56] J. P. Perdew, A. Zunger, “Self-interaction correction to density-functional approximations for many-electron systems”, Physical Review B, **23**, 5048 (1981)

[57] G. L. Oliver, J. P. Perdew, “Spin-density gradient expansion for the kinetic energy”, Physical Review A, **20**, 397 (1981)

[58] O. Gunnarson, B. I. Lunqvist, "Exchange and correlation in atoms, molecules, and solids by the spin-density-functional formalism", Physical Review B, **13**, 4274 (1976)

[59] A. D. Becke, "A new mixing of Hartree-Fock and local density functional theories", The Journal of Chemical Physics, **98**, 1372 (1993)

[60] J. Heyd, G. E. Scuseria, M. Ernzerhof, "Hybrid functionals based on a screened Coulomb potential", The Journal of Chemical Physics, **118**, 8207 (2003)

[61] J. P. Perdew, K. Burke, M. Ernzerhof, "Generalized Gradient Approximation Made Simple", Physical Review Letters, **77**, 3865 (1996)

[62] J. P. Perdew, M. Ernzerhof, K. Burke, "Rationale for mixing exact exchange with density functional approximations", The Journal of Chemical Physics, **105**, 9982 (1996)

[63] H.-P. Komsa, A. Pasquarello, "Assessing the accuracy of hybrid functionals in the determination of defect levels: Application to the As antisite in GaAs", Physical Review B, **84**, 075207 (2011)

[64] M. Kuisma, J. Ojanen, J. Enkovaara, T. T. Rantala, "Kohn-Sham potential with discontinuity for band gap materials", Physical Review B, **82**, 115106 (2010)

[65] O. Gritsenko, R. van Leeuwen, E. van Lenthe, E. J. Baerends, "Self-consistent approximation to the Kohn-Sham exchange potential", Physical Review A, **51**, 1944 (1995)

[66] A. H. MacDonald, W. E. Pickett, D. D. Koelling, "A linearised relativistic augmented-plane-wave method utilising approximate pure spin basis functions", Journal of Physics C, **13**, 2675 (1980)

[67] P. Błoński, S. Dennier, J. Hafner, "Strong spin-orbit effects in small Pt clusters: Geometric structure magnetic isomers and anisotropy", The Journal of Chemical Physics, **134**, 034107 (2011)

[68] D. Hobbs, G. Kresse, J. Hafner, "Fully unconstrained noncollinear magnetism within the projector augmented-wave method", Physical Review B, **62**, 11556 (2000)

[69] N. W. Ashcroft, N. D. Mermin, *Solid State Physics*, Saunders College Publishing, USA (1976)

[70] C. G. Van de Walle, J. Neugebauer, "First-principles calculations for defects and impurities: Applications to III-nitrides", Journal of Applied Physics, **95**, 3851 (2004)

[71] R. M. Nieminen, "Issues in first-principles calculations for defects in semiconductors and oxides", Modelling and Simulation in Materials Science and Engineering, **17**, 084001 (2009)

[72] M. Leslie, N. J. Gillan, "The energy and elastic dipole tensor of defects in ionic crystals calculated by the supercell method", Journal of Physics C: Solid State Physics, **18**, 973 (1985)

[73] G. Makov, M. C. Payne, “Periodic boundary conditions in *ab initio* calculations”, Physical Review B, **51**, 4014 (1995)

[74] A. Lindsay, E. P. O’Reilly, A. D. Andreev, T. Ashley, “Theory of conduction band structure of $\mathrm{InN}_x\mathrm{Sb}_{1-x}$ and $\mathrm{GaN}_x\mathrm{Sb}_{1-x}$ dilute nitride alloys”, Physical Review B, **77**, 165205 (2008)

[75] K. Laaksonen, H.-P. Komsa, E. Arola, T. T. Rantala, R. M. Nieminen, “Computational Study of $\mathrm{GaAs}_{1-x}\mathrm{N}_x$ and $\mathrm{GaN}_{1-y}\mathrm{As}_y$ alloys and arsenic impurities in GaN”, Journal of Physics: Condensed Matter, **18**, 10097 (2006)

[76] H.-X. Deng, J. Li, S.-S. Li, H. Peng, J.-B. Xia, L.-W. Wang, S.-H. Wei, “Band crossing in isovalent semiconductor alloys with large size mismatch: First-principles calculations of the electronic structure of Bi and N incorporated GaAs”, Physical Review B, **82**, 193204 (2010)

[77] L. Ivanova, H. Eisele, M. P. Vaughan, Ph. Ebert, A. Lenz, R. Timm, O. Schumann, L. Geelhaar, M. Dähne, S. Fahy, H. Riechert, E. P. O’Reilly, “Direct measurement and analysis of the conduction band density of states in diluted $\mathrm{GaAs}_{1-x}\mathrm{N}_x$ alloys”, Physical Review B, **82**, 161201 (2010)

[78] P. S. Dutta, H. L. Bhat, V. Kumar, “The physics and technology of gallium antimonide: An emerging optoelectronic material”, Journal of Applied Physics, **81**, 5821 (1997)

[79] D. Wang, S. P. Svensson, L. Shterengas, G. Belenky, C. S. Kim, I. Vurgaftman, J. R. Meyer, “Band edge optical transitions in dilute-nitride GaNSb”, Journal of Applied Physics, **105**, 014904 (2009)

[80] H. Bracht, S. P. Nicols, W. Walukiewicz, J. P. Silveira, F. Briones, E. E. Haller, “Large disparity between gallium and antimony self-diffusion in gallium antimonide”, Nature, **408**, 69 (2000)

[81] M. Hakala, M. J. Puska, R. M. Nieminen, “Native defects and self-diffusion in GaSb”, Journal of Applied Physics, **91**, 4988 (2002)

[82] G. Henkelman, H. Jónsson, “Improved tangent estimate in the nudged elastic band method for finding minimum energy paths and saddle points”, Journal of Chemical Physics, **113**, 9978 (2000)

[83] P. Erhart, D. Åberg, V. Lordi, “Extrinsic point defects in aluminum antimonide”, Physical Review B, **81**, 195216 (2010)

[84] V. Popescu, A. Zunger, “Effective Band Structure of Random Alloys”, Physical Review Letters, **104**, 236403 (2010)

[85] W. H. Press, S. A. Teukolsky, W. T. Vetterling, B. P. Flannery, *Numerical Recipes: the art of scientific computing*, Cambridge University Press, New York, 3rd ed. (2007)

Aalto-DD 13/2014

ISBN 978-952-60-5546-6
ISBN 978-952-60-5547-3 (pdf)
ISSN-L 1799-4934
ISSN 1799-4934
ISSN 1799-4942 (pdf)

Aalto University
School of Science
Department of Applied Physics
www.aalto.fi

BUSINESS +
ECONOMY

ART +
DESIGN +
ARCHITECTURE

SCIENCE +
TECHNOLOGY

CROSSOVER

DOCTORAL
DISSERTATIONS